Energy & Environmental Science

Accepted Manuscript

ROYAL SOCIETY OF CHEMISTRY

www.rsc.org/ees

Cite this: DOI: 10.1039/c0xx00000x

www.rsc.org/xxxxxx

ARTICLE TYPE

Hetero-Nanostructured Suspended Photocatalysts for Solar-to-Fuel Conversion

Yu-Peng Yuan,[a] Lin-Wei Ruan,[a] James Barber,[b,c] Say Chye Joachim Loo,[c]* and Can Xue[c]*

Received (in XXX, XXX) XthXXXXXXXXX 20XX, Accepted Xth XXXXXXXXX 20XX

DOI: 10.1039/b000000x

Converting solar energy into valuable hydrogen and hydrocarbon fuels through photocatalytic water splitting and CO_2 photo-reduction is highly promising in addressing the growing demand for renewable and clean energy resources. Developing efficient photocatalysts for solar-driven H_2 production and CO_2 reduction is the most essential part in achieving this goal. For the purpose of attaining high photocatalytic efficiency, hetero-nanostructures formed by multiple material components have been demonstrated as an effective strategy. Within this heterostructure, its interface is a critical consideration, whereby it determines the principle of charge transfer across the heterojunctions and consequent surface reactions. This article reviews the recent developments of hetero-nanostructures for photocatalytic H_2 production and CO_2 reduction based on material compositions that form heterojunctions.

1. Introduction

Human civilization is mainly powered by fossil fuels such as petroleum, coal and natural gas. The combustion of these fossil fuels has caused detrimental environmental pollution and enormous CO_2 emission. According to British Petroleum (BP) statistical review of world energy 2014, the worldwide energy consumption in 2013 has reached 533×10^{18} J, corresponding to an average energy consumption rate of 16.9 TW. Most of the energy consumed (>85%) comes from fossil fuels with 38% from oil, 27.3% from natural gas and 34.7% from coal. In 2013 alone, the burning of fossil fuels has resulted in unprecedented CO_2 emission of 36 billion tonnes (Gt).[1] In addition, the world energy consumption rate is projected to be ~27.6 TW by 2050, corresponding to more than 40.3 Gt CO_2 emission.[2] In order to meet the projection by the Intergovernmental Panel on Climate Change (IPCC) on carbon intensity (kg of C emitted to the atmosphere as CO_2 per year per W of power produced from the fuel) of ~ 0.45, significant contributions from carbon-free power resources are needed to substitute fossil fuels in total energy consumption.

The incident solar energy on the surface of the Earth is over 1.3×10^5 TW, far beyond the current global energy consumption rate (~16.9 TW in 2013) by roughly four orders of magnitude. Even though photovoltaic and electrochemical solar cells can reach high efficiency for solar energy conversion, many issues still remain unresolved, such as high fabrication costs, insufficient light harvesting, low output power density, and inconvenient transportation. Therefore, conversion of solar energy into transportable chemical fuels, such as methanol, methane and hydrogen fuels, by using sunlight, water and CO_2, is one of the most attractive routes since these are highly abundant on earth.

In principle, the generation of solar fuels can be achieved by using solar light to drive the reaction of proton reduction (eq. 1) or CO_2 reduction via different pathways (eq. 2-6) accompanied by a water oxidation process (eq. 7).[3] The redox potentials of these reactions are referred to NHE at pH=7.

$2H^+ + 2e^- \rightarrow H_2$	E^0 = -0.42 V	(1)
$CO_2 + 8H^+ + 8\ e^- \rightarrow CH_4 + 2\ H_2O$	E^0 = -0.24 V	(2)
$CO + 2\ H^+ + 2\ e^- \rightarrow CO + H_2O$	E^0 = -0.53 V	(3)
$CO_2 + 6\ H^+ + 6\ e^- \rightarrow CH_3OH + H_2O$	E^0 = -0.38 V	(4)
$CO_2 + 4\ H^+ + 4\ e^- \rightarrow HCHO + H_2O$	E^0 = -0.48 V	(5)
$CO_2 + 2\ H^+ + 2\ e^- \rightarrow HCOOH$	E^0 = -0.61 V	(6)
$2H_2O \rightarrow O_2 + 4H^+ + 4e$	E^0 = +0.81 V	(7)

The potential success of solar-to-fuels conversion relies on the development of efficient photocatalysts that absorb photon energy from sunlight to create active charge carries capable of implementing these redox processes towards hydrogen or carbohydrate fuels generation. A suitable semiconductor photocatalyst requires a sufficiently high conduction band (CB) edge to enable excited electrons to reduce water or CO_2 (eq. 1-6), and deep valance band (VB) level to allow the photogenerated holes to oxidize water (eq. 7).[4] Till now, more than a hundred types of semiconductor materials have been reported as possible photocatalysts for water splitting and CO_2 reduction.[5-9] However, most of these materials possess a fairly large bandgap, resulting in limited activity in the visible spectrum range that accounts for ~43% of solar energy.

Beside this, the overall efficiency of solar-to-fuels conversion over semiconductor photocatalysts is also determined by the separation of photogenerated electrons and holes as well as the

kinetics of surface redox reactions.[10-13] The fast recombination of photogenerated electrons and holes is one of dominant reasons that results in low photon conversion efficiency because the recombination process (~10^{-9} s) is much faster than surface redox processes (10^{-8}-10^{-1} s).

In view of this, researchers have now recognized that a single semiconductor alone is hardly competent for efficient solar fuels generation due to the great challenges of balancing the four parameters: 1) VB/CB levels; 2) light-harvesting capability; 3) electron-hole separation efficiency; 4) surface reaction rate. Therefore, it is desirable to form a hybrid photocatalyst consisting of semiconductor heterojunctions, which not only allows a broader range of solar light absorption but also significantly promotes the separation of photogenerated charge carriers, and thereby improving solar-to-fuel conversion efficiency.[14-17]

In the heterostructured semiconductor photocatalysts, the key issue is the interface between different components. Heterojunctions formed between different types of materials have different principles of charge transfer and consequent activities. Therefore, we have divided the discussion in this review based on the material compositions that form heterojunctions: semiconductor-semiconductor, semiconductor-co-catalyst, and semiconductor-metal. For solar-to-fuel conversion, we will focus mainly on photocatalysts in particular for H_2 production from proton reduction or CO_2 reduction without external electric field, since there already have been a number of recent reviews on heterojunction-based photoanode or photocathode for photoelectrochemical (PEC) cell. [18-20]

2. Semiconductor-semiconductor heterostructures

2.1 Design strategy: promoting interfacial charge separation

The idea of forming semiconductor heterojunctions relies on the band energy alignment between the two semiconductors at the interface. For example, figure 1 shows the band alignment and bending at the heterojunctions created by two n-type semiconductors with different band energy position and Fermi level. Once the junction is formed, electrons will flow from the semiconductor with higher Fermi energy level (semiconductor **I**) to the semiconductor with lower Fermi level (semiconductor **II**), which results in an electron-depletion region in semiconductor I and an electron-accumulation region in semiconductor II. This creates a built-in electric field at the interface with a potential difference between the two sides. The electron flow will stop when the Fermi levels on both side become equal. Consequently, equilibrium is established at the heterojunction with a built-in voltage of eV_b (E_{f1}-E_{f2}). The energy difference between the interface and the bulk in semiconductor due to electron flow causes the band bending upward or downward.

Yu-Peng Yuan is a faculty staff at Anhui University. He received his BE and ME degrees from Hefei University of Technology and PhD degree from Nanjing University. He worked as a Research Fellow at Nanyang Technological University in 2012-2013. His current research interests focus on interfacial chemistry, gas adsorption, chemistry of materials, and first principle calculations.

Lin-Wei Ruan is currently a graduate student in School of Chemistry and Chemical Engineering at Anhui University where he obtained his Bachelor of Engineering in 2008. He is doing his research with Dr. Yu-Peng Yuan on molecular simulations and first principles calculations.

Jamaes Barber is the Ernst Chain Professor of Biochemistry at Imperial College London and is a Fellow of The Royal Society of London and Royal Society of Chemistry. He is also a visiting professor at Nanyang Technological University and Lee Kuan Yew Distinguished Visitor to Singapore. He has been awarded several medals and prizes for his contributions to understanding the molecular processes of photosynthesis.

Joachim Loo is associate professor in the School of Materials Science and Engineering (MSE) and the Singapore Centre on Environmental Life Sciences Engineering (SCELSE) at Nanyang Technological University (NTU) in Singapore. He is also Director of the NTU Solar Fuels Laboratory. His research interest lies in materials for energy, environmental and biomedical applications, and has filed several patents in this field. In 2012, he was awarded the Outstanding Mentor Award and the Nanyang Award for Excellence in Teaching. He is also Assistant Chair (Students) in MSE, and a committee member of the ISO/TC 229 Nanotechnology National Working Group in Singapore.

Can Xue is an assistant professor in the School of Materials Science and Engineering at Nanyang Technological University. He received his BS degree at University of Science and Technology of China in 2002, and obtained PhD degree at Northwestern University (IL, US) in 2007. He has been awarded the Lee Kuan Yew Research Fellowship in 2008. His current research interests focus on the development of new plasmonic metal nanostructures and metal-semiconductor hybrid nanostructures for photocatalytic applications.

Depending on the bandgap and relative energy level of the CB and VB, the semiconductor heterojunctions can be divided into three categories: straddling gap (type 1), staggered gap (type 2) and broken gap (type 3), as shown in Fig. 2. For type 1 heterostructure, the CB and VB levels of the larger bandgap semiconductor straddle that of the narrower bandgap semiconductor. For type 2 junction, the CB and VB levels are staggered between two semiconductors. For type 3 junction, the CB level of semiconductor II lies below the VB level of semiconductor I.

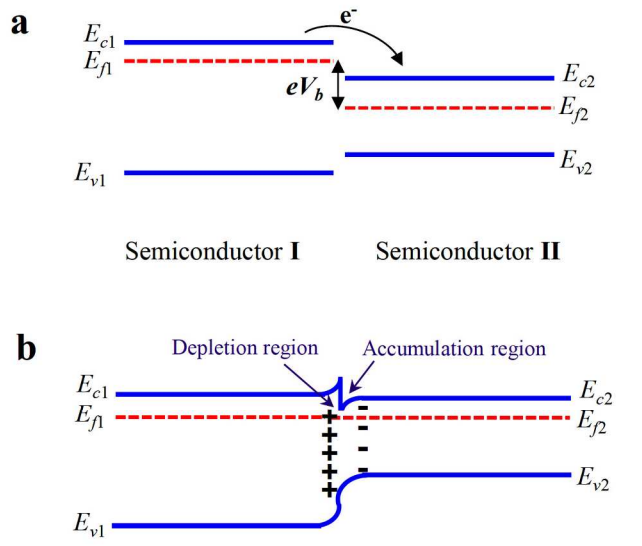

Fig. 1 Diagram of a typical n-n type heterojunction: (a) in contact (b) in equilibrium.

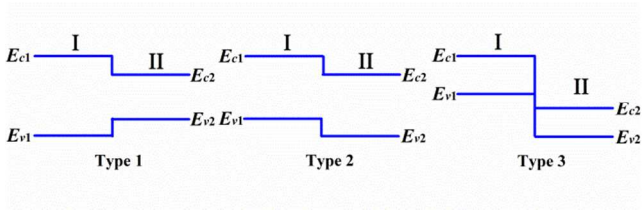

Fig. 2 Energy diagrams for three different types of heterojunctions

By choosing appropriate semiconductors, the obtained hetero-nanostructured photocatalysts can not only gain wider spectral range of light absorption but also improve the separation of the photogenerated electrons and holes. In the past several decades, development of heterostructured photocatalysts has received tremendous interests for enhancing solar-to-fuel conversion efficiency.[16, 21, 22] However, we have to point out that interfacial electron and/or hole transfer would possibly decrease the reducing ability of the excited electrons and oxidation ability of the holes. For example, even though more efficient charge separation can be achieved from the Cu_2O-TiO_2 heterostructure, it showed lower activity for Orange II degradation as compared to pure TiO_2 under UV-vis light irradiation due to the lowered oxidation ability of holes in Cu_2O.[23] Therefore, in order to obtain high photocatalytic efficiency, especially for proton reduction or CO_2 reduction that requires high reduction potentials, the band energy level and charge separation are equally important considerations. In addition, the effectiveness of electron/hole migration may also be influenced by the potential wells and barriers at the heterojunction,[24] particle size and morphology, crystal phase and facets, and surface reactivity,[22] all of which should be considered in designing heterostructured semiconductor photocatalysts.

In the fabrication of hetero-structured photocatalysts, the most common strategy is through in-situ growing of one material onto the other material as the "base" or substrate. Therefore, the morphology and structure of the "base" material would have strong impact on the growth process of the growing materials as well as the activities of resultant heterojunctions. For example, if the "base" material exhibits two-dimensional (2D) structure with excellent charge transport ability, it would allow for controllable growth of the second photocatalyst on its surface with improved charge separation across the generated heterojunctions. Moreover, if the growing second material uniformly covers the base material, it would form a core-shell heterostructure with large interfacial area that enables more efficient charge separation as compared to regular particle-particle junctions. Therefore in this section, we will discuss the semiconductor heterojunctions based on the geometrical configuration of the heterostructure, including particle-particle junction, particle-on-2D junction, and core-shell heterojunction. For particle-particle junction, the homo-junctions composed by the same compound with different band levels will be discussed in a separate sub-section due to their unique structural features.

2.2 Homo-junction of the same compound

It is known that for semiconductor nanostructures, the band energy levels are highly dependent on the crystal phase. Therefore, heterojunctions can be formed between different phases of one type of semiconductor with the same chemical composition. By this way, charge separation can be promoted by the slight band alignment between different phases across the heterojunction.

A typical example is TiO_2 which has three major crystalline phases: anatase, rutile, and brookite. In particular, the anatase and rutile phases have been extensively explored for photocatalytic applications. Due to their large bandgap (rutile:~3.0 eV; anatase:~3.2 eV),[25-27] pure TiO_2 can only act as photocatalyst under UV-light excitation, and most of the photogenerated electrons and holes usually recombine within a few nanoseconds. Consequently the available charge carriers for surface redox reactions are limited.[28, 29] However, researchers have recognized that creating TiO_2 phase junctions can be an effective strategy for improving charge separation. The most famous example is Degussa P25, a highly benchmarked photocatalyst containing anatase (75 wt%) and rutile (25 wt%) TiO_2, which shows notably higher photocatalytic efficiency than that of the single phase anatase or rutile TiO_2 due to the large junction area between the two phases, and with a relatively more efficient charge separation.[30,31] Furthermore, with appropriate thermal treatment of P25, Li *et al.* found that the rutile content in P25 can be tuned to achieve 3-5 times higher photocatalytic activity for H_2 production from biomass reforming. [32]

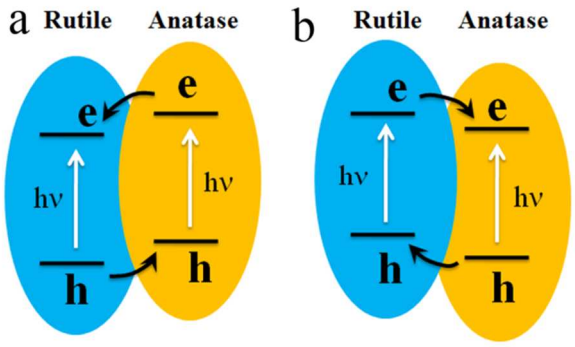

Fig. 3 Schematic illustration of anatase-rutile TiO_2 phase junction for electron-hole separation and electron transfer from (a) anatase to rutile,[33] and (b) rutile to anatase.[34]

Nevertheless, there have been debates on how the bands align between anatase and rutile TiO_2. Since 1996 when Kavan *et al.* reported that the flatband potential of anatase (101) is ~0.2 eV more negative than that of rutile (001),[33] many researchers have consented that the CB of anatase is ~0.2 eV higher than that of rutile, which allows photogenerated electrons to transfer from anatase to rutile and the holes similarly migrate in the reverse direction (Fig. 3a). However, recent XPS studies by Scanlon *et al.* indicated that the VB of anatase lies ~0.4 eV lower than that of rutile and its CB is ~0.2 eV higher than the rutile CB (Fig.3b),[34] in which case its charge transfer direction is opposite.

Another phase, brookite TiO_2, received less attention in the past decades because it is generally considered to have low photoactivity. But Ohno *et al.* recently showed that brookite TiO_2 nanorods with large (210) facets are quite active for photocatalytic CO_2 reduction into methanol.[35] Similar to P25, the mixed TiO_2 phases of brookite with anatase and/or rutile were also found to exhibit high photocatalytic activity.[36-39] Bahnemann *et al.* demonstrated that the TiO_2 mixtures of brookite nanorods and anatase particles exhibited higher photocatalytic H_2 generation rate from methanol solution than pure anatase TiO_2 particles due to the higher CB (~0.14 eV) of brookite to anatase.[36] Tay *et al.* also reported similar phenomenon and proved the transfer of photogenerated electrons from brookite to anatase through transient absorption (TA) spectroscopy.[40] Interestingly, Huang *et al.* found that triple-phase composites of TiO_2 can exhibit about four times higher activity in photocatalytic H_2 production than P25 because the additional anatase-brookite junctions allow for more efficient charge separation.[41] However, brookite-rutile junctions showed relatively weaker activity as compared to the single phase anatase or rutile probably because the brookite phase is not active for H_2 evolution.

Besides TiO_2, some other phase junctions have also been explored recently. Li *et al.* reported the junction of α-Ga_2O_3 and β-Ga_2O_3which was constructed through phase transformation from α-Ga_2O_3 through heat treatment.[42] The prepared α-β-Ga_2O_3 junctions exhibited enhanced photocatalytic activity as compared to the pure α- and β-Ga_2O_3 for overall water splitting under UV-light irradiation. This was due to band alignment at the α-β-Ga_2O_3 heterojunction resulting in more efficient interfacial charge separation.[42] By using the molten salts method, Wark *et al.* presented the preparation of a series of phase junctions of calcium tantalate (cubic α-$CaTa_2O_6$, orthorhombic β-$CaTa_2O_6$, etc.).[43] These composites with mixed phase junctions showed high activity for photocatalytic H_2 generation in methanol solution without any co-catalyst. This is attributed to significantly improved separation of photoexcited charge carriers at the interface of the different phases. Guo *et al.* recently demonstrated twin-induced phase junction in $Cd_{0.5}Zn_{0.5}S$ nanorods which exhibited alternating zinc-blende (ZB) and wurtzite (WZ) segments along [111] direction.[44] The type-II staggered band alignment formed at the ZB-WZ junctions, resulted in highly efficient charge separation and a remarkable quantum efficiency of 62% in photocatalytic H_2 production.

In addition to phase difference, vacancy sites could also lead to a variation of the electronic structure of the semiconductor compound. A representative example is Cu_2O which is a typical p-type semiconductor due to the dominant Cu vacancies. However, some researchers reported that the preparation of n-type Cu_2O in acidic solution might favour the generation of oxygen vacancies though the nature of n-type Cu_2O, though this is still under much debate.[45] If so, the heterojunction of p-n Cu_2O can be fabricated to promote the separation of photogenerated charge carriers and consequently improve photocatalytic activity.[46, 47]

Comparing to natural vacancies in the crystal structure, artificial doping by the additional of other elements is a more popular option to adjust band structures of semiconductors. This allows for heterojunction formation of the same compound but with different types of doping. For example, TiO_2 is an n-type semiconductor, but by creating Ti vacancies at elevated temperature and pressure,[48] or doping with low valence ions, such as Fe^{3+},[49, 50] Co^{3+},[51] Cr^{3+},[52] V^{3+},[53] p-type TiO_2 structures have been obtained and extensively studied for photocatalytic applications. Heterostructured hybrids by integrating n-type and p-type TiO_2 have been demonstrated to assist the charge carrier separation for enhanced photocatalytic activities.[54, 55]

2.3 Nanoparticle-heterojunctions between different semiconductors

In the past decade, a number of hetero-nanostructure photocatalysts composed of different semiconductor combinations have been reported due to their relatively more effective charge separation at the interfaces, as compared to their individual component. In particular, for the purpose of CO_2 reduction or H_2 generation via proton reduction, both semiconductors must have CB levels sufficiently higher than the redox potential of these two representative reactions. Therefore, some metal oxides, including TiO_2, ZnO, In_2O_3, etc., have been widely used as the base materials to couple with another semiconductor nanostructure of a higher CB level to form heterojunctions. However, these metal oxides usually have large bandgaps and very limited visible-light activity. Thus, they are usually coupled with relative narrow bandgap semiconductors which can effectively be excited by visible-light and are capable of injecting photogenerated electrons into the CB of the contacting metal oxides for reduction reactions.

TiO_2, as the most common base photocatalyst with excellent stability, has been used to form heterostructures with CdS,[56-59] $TiSi_2$,[60] CuO,[61, 62] In_2S_3,[63] for photocatalyticH_2 generation, and with CdSe,[64] AgBr,[65] PbS,[66] for CO_2 photoreduction. Among

them, CdS or CdSe decorated TiO_2 structures have received lots of attention due to the perfect band alignment with the highly efficient electron transfer from CdS/CdSe to TiO_2 under visible light excitation. For example, Wang *et al.* employed CdSe quantum dots to sensitize platinized TiO_2 (P25). Although the CB edge of bulk CdSe is only slightly higher than that of TiO_2, the quantum confinement can shift it to a higher level. As a result, the photoinduced electrons are injected from CdSe quantum dots into TiO_2, and this heterojunction is capable of catalyzing the photoreduction of CO_2 into CH_4 and CH_3OH under visible light irradiation.[64]

Till date, a variety of TiO_2 nanostructures, including nanotube and nanotube arrays,[67-73] branched TiO_2,[74] hollow sphere,[75] and nanowires[76, 77] nanosheets,[78] have been decorated with CdS or CdSe for improved solar-to-hydrogen generation. In particular the one-dimensional TiO_2 nanostructures, such as nanowires and nanotubes, can exhibit excellent efficiency in PEC after decorated with CdS or CdSe quantum dots, which benefits from the vectorial electron transport within the TiO_2 structure (Fig. 4). [79-81]

However, unlike the organic dye-sensitized metal oxide in which the photogenerated electrons can quickly transfer into the metal oxide, trap-state Auger recombination at the interface of QDs and metal oxide may result in the slow electron injection with high charge recombination rates, which decreases the photocatalytic efficiency.[82, 83] To solve this problem, ternary heterostructures consisting of QDs, Au nanoparticles, and metal-oxide semiconductor have been constructed with improved photocatalytic efficiency.[83-87] For example, Wu et al. have demonstrated that the Au nanoparticle decorated between CdS QDs and TiO_2 nanorod can serve as an electron relay to facilitate the charge transfer between photoexcited CdS and TiO_2, which increases the charge-transfer lifetime, reduces the trap-state Auger rate.[83]

An alternative to improve the activity is enhancing light harvesting. Ding *et al.* demonstrated that the butterfly wing architectures of TiO_2 can effectively reduce 40% reflection of UV light. The resulted CdS-TiO_2 heterostructures exhibited improved H_2 generation efficiency by 200% as compared to plate-like TiO_2.[88] Besides TiO_2, ZnO and In_2O_3 have also been widely used to form heterojunctions with other semiconductors for photocatalytic H_2 production, including ZnSe-ZnO,[89] CdS-ZnO,[90, 91] ZnS-ZnO,[92] CuO-ZnO,[93] $CuInS_2$-ZnO,[94] In_2O_3-$NaNbO_3$,[95] $Gd_2Ti_2O_7$-In_2O_3,[96] and so on.

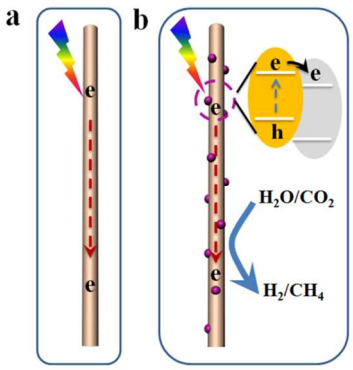

Fig. 4 Schematic illustration of charge vectorial transfer in (a) 1-D TiO_2 nanostructure and (b) quantum dot sensitized 1-D TiO_2 nanostructure for H_2 generation and CO_2 reduction.

In order to achieve suitable band alignment, doping is usually a favorable strategy to tune the band structures of semiconductors. For example, the Cr-doped $Ba_2In_2O_5$-In_2O_3 heterojunctions can be used for H_2 generation in methanol solution under visible light irradiation, and overall water splitting under UV light irradiation.[97] The appropriate Cr-doping allows perfect band alignment between $Ba_2In_2O_5$ and In_2O_3 with effective separation of photogenerated electrons and holes, which enables redox reactions to occur separately on the surface of Cr-In_2O_3 for H_2 evolution and on Cr-$Ba_2In_2O_5$ surfaces for O_2 evolution. Li *et al.* showed that Zn-doping of β-Ga_2O_3 resulted in the formation of $ZnGa_2O_4$–β-Ga_2O_3 heterojunctions with a type-2 band alignment, which facilitated charge separation and enhanced photocatalytic activity for water splitting. [98]

Previously, most reported heterostructured photocatalysts are constructed between two n-type semiconductors, even though a p-n junction is known to be more effective in charge separation due to the built-in electric field. Examples of p-n heterojunction photocatalysts are much fewer because p-type semiconductors are rather rare in nature as compared to the n-type semiconductors. Lee *et al.* have demonstrated that through a hydrothermal process, p-type $CaFe_2O_4$ nano-islands can be created on then-type $PbBi_2Nb_{1.9}W_{0.1}O_9$ particles to form p-n heterojunctions that are capable for both H_2 production in methanol solution and water oxidation to O_2 in $AgNO_3$ solution under visible light irradiation (Fig.5).[99] A similar p-n nanojunction of $CaFe_2O_4$-$MgFe_2O_4$has also been constructed for improved photocatalytic H_2 production in isopropanol solution.[100] Following this work, Kim *et al.* fabricated a heterojunction photoanode of p-$CaFe_2O_4$/n-TaON that exhibited five times enhancement in PEC.[101]

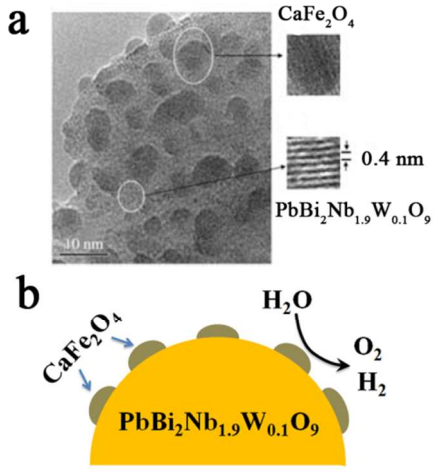

Fig. 5 (a) HRTEM image of $CaFe_2O_4$-$PbBi_2Nb_{1.9}W_{0.1}O_9$ p-n heterojunction. (b) schematic illustration of $CaFe_2O_4$-$PbBi_2Nb_{1.9}W_{0.1}O_9$ p-n heterojunction for H_2 and O_2 production. Reprinted with permission from Ref.99. Copyright 2005, Wiley.

In addition to metal oxides, some metal sulphides have also been used to form p-n junctions for photocatalytic applications. Yu *et al.* showed that by depositing p-type NiS nanoparticles onto n-type CdS nanorods, the resulted p-n hetero-nanostructures can exhibit even higher H_2 generation rate than 1 wt% Pt-loaded CdS nanorods under visible-light irradiation.[102] However, in the heterostructures of metal sulphides, cation-diffusion between

segments of different segments may have a negative effect on photoactivity. Mokari *et al.* demonstrated that p-type Cu_2S can be created on the tip of n-type CdS nanorods through cation exchange to form heterojunctions.[103] However, Cu^+ ions are able to diffuse into CdS lattice and act as a recombination center, which decreases the exciton lifetime in the nanorod. As a result, the p-Cu_2S/n-CdS hetero-nanorods showed even lower photocatalytic activity than the plain CdS nanorods.

Nevertheless, the presence of Cu^+ in some heterostructures based on CuO or Cu_2O may provide positive contributions to the photoactivity.[61, 104] For example, Xu *et al.* have shown that CuO-loaded TiO_2 could exhibit higher activity for H_2 production than Pt- or Pd-loaded TiO_2.[61, 105] Recently Durgakumari *et al.* also reported a very high H_2 production rate over CuO quantum dots decorated TiO_2 nanotubes under solar light irradiation,[106] and proposed that the electrons transferred from photoexcited TiO_2 will accumulate on CuO, leading to formation of Cu_2O thus facilitating the interfacial electron transfer to the proton in solution for H_2 evolution.

2.4 Heterojunctions on 2-D nanomaterials

Graphene, as a typical two-dimensional (2-D) nanomaterials composed of a single layer or a few layers of sp^2-hybrid carbon atoms, exhibits high specific surface area and outstanding thermal, mechanical, optical, and especially electrical properties.[107, 108] The 2-D structure of graphene with large surface area allows it to serve as an excellent platform for supporting semiconductor nanoparticles. In addition, the work function of graphene is -4.42 eV, which is slightly higher than that of H^+/H_2 reduction potential.[109-111] Thus, when a semiconductor particle with suitable CB position is deposited onto the graphene surface, the injection of photoexcited electrons from the deposited semiconductor particle to graphene would be thermodynamically favored. Moreover, graphene possesses excellent electronic conductivity and high mobility of charge carriers, thus the injected electrons can readily be transported along the graphene surface and collected for reduction reactions.[112, 113] For example, by using transient absorption spectroscopy and time-domain terahertz spectroscopy, Meng et al. have demonstrated that graphene can extract the photogenerated electrons from the α-Fe_2O_3 nanoparticles decorated on its surface, which increases the lifetime of charge carriers and thereby improving the photocatalytic activity.[114]

Due to the challenges in bulk-scale preparation of pristine graphene, most researchers synthesize graphene oxide (GO) based on Hummers' method, and treat it with different reducing agents to achieve a format of reduced graphene oxide (r-GO). Graphene oxide also exhibits semiconductor characteristics with tuneable bandgap depending on the oxidation degree or oxygen concentration in the structure,[115] and has been used as a photocatalyst for H_2 generation in methanol solution.[116] Although perfectly reduced graphene oxide without vacancy defects should be infinitely close to pristine graphene and gapless, the actual r-Go reported in literatures usually possess a small bandgap down to 1 eV.[117] As such, in the past five years, GO and r-Go have been extensively used as 2-D substrates to form heterojunction coupling various semiconductor nanostructures to achieve enhanced photocatalytic activities for H_2 generation and CO_2 reduction.

The first example presented by Zhang *et al.* was the decoration of TiO_2 particles onto r-GO surfaces, and the resulting TiO_2/r-GO composite showed higher H_2 generation rate in Na_2S and Na_2SO_3 solution than pristine TiO_2 and P25.[118] The excellent electronic conductivity of graphene enables rapid transportation of the injected electrons from TiO_2, thus promoting charge separation and photocatalytic activity. Following this work, other groups have also reported different heterostructures constructed by r-GO with TiO_2 nanowires,[119] nanosheets,[120] and nanotubes,[105] respectively, which all exhibited enhanced photocatalytic activity in H_2 production as compared to individual TiO_2 structures.

Compared to TiO_2, CdS is more photoactive in the visible region, and has a direct bandgap allowing for a more efficient charge injection. As such, researchers have made lots of efforts to fabricate heterojunctions of r-GO with CdS-based nanocrystals. For example, Gong *et al.* have prepared CdS cluster-decorated r-GO through a solvothermal method.[121] The resultant heterojunctions showed~5 times higher H_2 production rate than CdS nanoparticles alone. As illustrated by Fig. 6, the increased photocatalytic activityis attributed to the efficient electron collection by r-GO, which prolongs the lifetime of the photoinduced charge carriers from CdS. Jia *et al.* showed that comparing with undoped r-GO, N-doped r-GO could further improve H_2 generation activity upon coupling with CdS.[122] In addition, the electrons captured by graphene can readily be transported along r-GO surfaces to the nearby Pt co-catalyst for water reduction. Similar results of enhanced H_2 production have also been achieved by coupling r-GO with $Zn_xCd_{1-x}S$,[123] $Zn_{0.5}Cd_{0.5}S$ porous nanosheets,[124] ZnO-CdS,[125] MoS_2,[126] and SiC.[113,115] In addition, the reduction level of GO also strongly influences its activity. Fu *et al.* found that for the heterostructure formed by $ZnIn_2S_4$ and r-GO, the higher the reduction level of GO, the better H_2 generation rate was achieved, suggesting that the electron transport ability on graphene sheets plays a dominant role on the efficiency of charge separation over the heterostructures.[127]

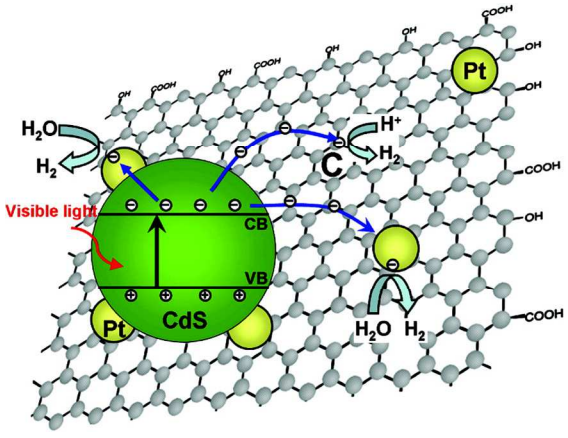

Fig. 6 Schematic illustration of the charge separation and transfer in the graphene-CdS system under visible light. Reprinted with permission from Ref.121. Copyright 2011, American Chemical Society.

Besides H_2 production, photoreduction of CO_2 has also been demonstrated by using graphene-based heterostructures. For example, through layer-by-layer (LBL) assembly of $Ti_{0.91}O_2$

nanosheets and GO sheets onto a polymer sphere followed by microwave treatment, the $Ti_{0.91}O_2$/r-GO hollow sphere junction could be prepared and showed much higher activity for photocatalytic CO_2 reduction than pure $Ti_{0.91}O_2$ and P25.[116] The enhancement arises from the intimate contact of $Ti_{0.91}O_2$ nanosheets with r-GO as well as the hollow sphere structure that facilitates light absorption via multi-scattering process. Zou *et al.* showed that by introducing Ti^{3+} to TiO_2/r-GO hybrids with ethylenediamine as the reducing agent, selective conversion of CO_2 to CH_4 and C_2H_6 could be achieved in the presence of water vapour because Ti^{3+} favours coupling photo-generated $\cdot CH_3$ radicals into C_2H_6.[128] This work provides a new strategy for C-C catalytic reaction over graphene-based photocatalysts. More recently, Yu *et al.* prepared CdS nanorod/r-GO heterostructures through a one-step microwave-hydrothermal process, which showed over 10 times higher CH_4 production rate than pure CdS, and better than Pt loaded CdS.[129] It was believed that r-GO can not only enhance the adsorption and activation of CO_2, but also generate photo-excited electrons, thus resulting in enhanced CO_2 reduction over the CdS/r-GO photocatalyst. It is noteworthy that defects on r-GO could have negative effects on its photocatalytic activity. Hersam *et al.* have compared P25/r-GO with P25/SEG (solvent exfoliated graphene) for CO_2 photoreduction, and demonstrated that the former exhibited significantly lower methane production rate than the latter.[130] This observation again proves the high importance of charge transport on graphene to the performance of graphene-based heterostructures.

Graphitic carbon nitride (g-C_3N_4) is another type of two-dimensional material with a bandgap of 2.4~2.8 eV,[131, 132] and can be synthesized through calcination of some molecular precursors such as melamine,[133] urea,[134-136] and cyanamide.[137] The raw g-C_3N_4 obtained right after calcination usually appears like a bulk crystal with random shapes, but one can easily exfoliate it into very thin nanosheets through ultrasonication in an appropriate chemical environment.[138] Owing to its visible-light activity, high stability and suitable band levels capable for water splitting, g-C_3N_4 has attracted tremendous interest for photocatalytic applications in the past five years. However, individual g-C_3N_4 usually encounters problem of rapid recombination of photogenerated electrons and holes. Therefore, efforts have been made to couple g-C_3N_4 nanosheets with other materials, including graphene,[139-142] TiO_2,[143-145] ZnO,[146, 147] In_2O_3,[148] CdS,[149-151] and TaON,[152] in order to achieve more efficient charge separation and enhanced photocatalytic activity for H_2 generation and CO_2 reduction.

The heterojunction formed between two inorganic 2-D structures has also been explored. For instance, Ida *et al.* reported an ultrathin p-n junction by depositing nanosheets of p-type NiO and n-type calcium niobate (CNO) sequentially on a quartz substrate.[153] The prepared CNO/NiO (n−p) junction films showed two times higher rate of photocatalytic H_2 generation than the individual n-CNO film and p-NiO film.

2.5 Core-shell heterojunctions

As stated earlier, the interface area of heterojunctions is critical in determining the final photocatalytic efficiency. In order to achieve large interface area, a core-shell structure is often a more favourable approach as opposed to normal hetero-nanoparticles. In recent years, there are growing interests on the development of core-shell hetero-nanostructures for solar-to-fuel conversion.

For one-dimensional (1-D) semiconductor nanostructures, i.e. nanowires and nanotubes, which can be grown on a conductive substrate surface, creating core-shell junctions not only enables effective charge separation, but also can take advantage of vectorial charge transport along the 1-D structure. Therefore, a number of 1-D core-shell photoelectrodes, such as TiO_2-coated Cu_2O/CuO coaxial nanocables,[154] CdSe sensitized CdS@ZnO nanowires,[155] α-Fe_2O_3/graphene/$BiV_{1-x}Mo_xO_4$ nanorods,[156] Si@ZnO nanowires,[157] cobalt-doped α-Fe_2O_3@ $MgFe_2O_4$ nanorods,[158] Si/InGaN hierarchical nanowire arrays,[159] have been reported for PEC water splitting.

In comparison, for photocatalytic systems without external circuit to drive the charge carriers, redox reactions occur on the surface of both core and shell materials especially for type-II heterojunctions of core-shell structures. As such, the shell layer is usually porous or does not fully cover the core structure. For example, Fang *et al.* reported that hollow SnO_2@SiC core-shell spheres showed enhanced photocatalytic activity in H_2 evolution due to both interfacial charge separation and the porous structure.[160] Another representative example was reported by Yu *et al.* on CdS@g-C_3N_4 core-shell nanowires that were prepared by suspending CdS nanowires and g-C_3N_4 thin nanosheets into methanol followed by a slow drying process (Fig. 6).[161] With a small amount of surface g-C_3N_4, there were some uncovered sites of the CdS nanowire surfaces allowing for effective charge separation at the CdS/g-C_3N_4 heterojunctions, and more importantly H_2 evolution on the CdS surface. As such, the resulting CdS@g-C_3N_4 core-shell nanowires showed twice higher H_2 generation rate than pure CdS nanowires without shell (Fig. 7a). However, at high concentration of g-C_3N_4 in the suspension, a dense and closed g-C_3N_4 shell covering the entire CdS nanowire surface leads to significant decrease in photocatalytic activity (Fig. 7b).

However, the situation is different and somewhat surprising for type I core-shell structures that can also exhibit enhanced photocatalytic activity. For example, theoretically, in CdSe@CdS core-shell nanocrystal, as a type-I junction, photogenerated electrons and holes could be transported together towards the CdSe core, and the CdS shell acts as a physical barrier that inhibits access of photogenerated electrons to the nanocrystal surface, which should decrease the activity for photocatalytic reactions (Fig. 8a). However, Larsen *et al.* observed a 10-fold increase in photocatalytic H_2 generation over the CdSe QDs passivated by a very thin layer of CdS shell as compared to the bare CdSe QDs.[162] Similar phenomenon was also reported by Li *et al.* on the CdS@ZnS core-shell nanocrystal which showed much higher activity in photocatalytic H_2 production than the CdS nanocrystal alone.[163] It was proposed that the enhanced photoactivity of such type-I core-shell nanocrystals is attributed to the fast tunnelling of photogenerated electrons from the core to the shell surface (Fig. 8b), or electrons leaking from the uncovered core surface in the case of a very thin shell. In addition, shell passivation would prevent photocorrosion of the unstable core, which might be another reason for the improved activity. In contrast, Lee *et al.* reported an inversed-type I structure, In_2O_3-In_2S_3 core-shell nanorods, with enhanced H_2 production in methanol solution under UV-vis light irradiation.[164]

In this case, the wide band gap In_2O_3 nanorod core was covered by In_2S_3 nanoflakes with narrow band gap, which enables photoexcited electrons and holes in the In_2O_3 core to migrate towards the In_2S_3 shell surface for direct redox reactions.

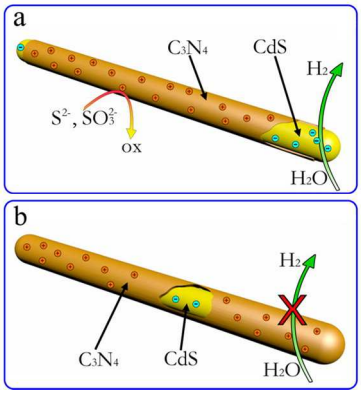

Fig. 7 Schematic illustration of photocatalytic H_2 production over aCdS nanowire partially covered g-C_3N_4 (a) or fully covered CdS nanowire (b). Reprinted with permission from Ref. 161. Copyright 2013 American Chemical Society.

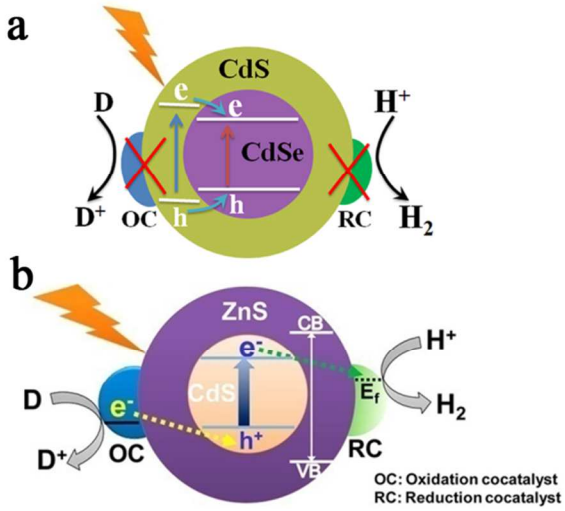

Fig. 8 (a) Theoretical charge transfer process in CdSe@CdS type I core-shell structure with decreased photocatalytic activity. (b) The proposed principle for CdS@ZnS structure with actually enhanced photocatalytic activity. Reprinted with permission from Ref. 163. Copyright 2013 American Chemical Society

3. Heterojunctions of semiconductor photocatalyst and noble-metal-free co-catalysts for H_2 evolution

For most semiconductor photocatalysts, the overpotentials on the surfaces for hydrogen evolution reaction (HER) are always a critical issue that restricts the overall photocatalytic efficiency of water splitting. It is common to deposit noble metals (e.g. Pt, Pd, Au etc.) to lower the overpotential and enhance efficiency. Nevertheless, due to the high cost of noble metals, researchers are making efforts to use cheap noble-metal-free co-catalysts with high efficiency for H_2 evolution. By coupling the co-catalyst with the semiconductor photocatalyst, it forms a different type of heterojunction as compared to semiconductor-semiconductor and metal-semiconductor junctions in terms of the nature and principle of interfacial charge transfer.

Some transition metal sulphides, oxides, and complexes have been found to be effective co-catalysts that can extract photoexcited electrons from the semiconductor photocatalyst for efficient proton reduction in H_2. But these co-catalyst compounds alone are not photoactive for H_2 generation. In this section, we will review recent developments on heterojunctions of semiconductor-co-catalyst for photocatalytic H_2 production based on the composition of the metal compound co-catalyst.

3.1 Transition metal oxide-semiconductor heterojunctions

Over the past several decades, some metal oxides such as RuO_2,[165, 166] Cr_2O_3,[155] $Rh_{2-y}Cr_yO_3$,[16,157] CoO_x,[167] have been used to deposit onto photocatalyst surfaces as co-catalysts for oxygen evolution reaction (OER) to promote photocatalytic efficiency for overall water splitting. However, for metal oxide co-catalyst for H_2 evolution, there are fewer of such examples reported.

A well-recognized example is NiO which has been used for promoting H_2 production for many years. An appropriate reduction-oxidation process is usually needed to achieve high H_2 production rate when NiO_x is used as co-catalyst.[168, 169] It is believed that the reduction process converts the loaded NiO_x particle into metallic Ni, on which the outmost layer would be subsequently oxidized back to NiO again. As a result, the so called NiO_x co-catalyst is in fact composed of a Ni core with a very thin layer of NiO shell. Such Ni-NiO core-shell structures created on the surfaces of semiconductor photocatalysts could not only improve photocatalytic H_2 production but also suppress the back reaction of H_2 and O_2 into H_2O.[170] However, a recent study by Osterloh *et al.* indicates that NiO_x-loaded $SrTiO_3$ photocatalyst behaves more like a three component Ni-$SrTiO_3$-NiO structure that allows for proton reduction and water oxidation to occur on Ni and NiO, respectively.[153] A separate study by Hwang *et al.* also showed that the Ni/NiO co-loaded GO exhibits higher activity for H_2 generation than NiO-loaded GO,[154] implying that the metallic Ni may have considerable contribution to the enhanced H_2 evolution by NiO_x.

3.2Transition metal sulfide-semiconductor heterojunctions

Comparing to metal oxides, transition metal sulphides are more capable of acting as HER co-catalysts when coupled with semiconductor photocatalysts for H_2 production.[132-146] The first example was reported by Li *et al.* in 2008 on the MoS_2-loaded CdS that showed 36 times higher H_2 production rate than CdS alone,[171] while MoS_2 alone is not photoactive for H_2 generation. The intimate contact between MoS_2 and CdS enables the electron transfer from photoexcited CdS to MoS_2, and more importantly, MoS_2 provides catalytically active sites,[172, 173] allowing the received electrons for efficient proton reduction. Similar to MoS_2, WS_2 belonging to the same group was found to have similar function for improved H_2 production when coupled with CdS.[174]

Apart from sulfide-sulfide contact, MoS_2can also be coupled with non-sulfide photocatalysts for improved H_2 generation owing to the benefit of its surface active sites for HER. Zhang *et al.* have demonstrated that a few layered MoS_2 nanosheets can grow onto TiO_2 nanobelts, which creates a heterostructures

showing high efficiency for photocatalytic H_2 production. Hou *et al.* have reported layered nanojunction between MoS_2 and mesoporous g-C_3N_4 that improves H_2 production.[175] The very thin layered MoS_2 with anisotropic conductivity promoted charge transport between different layers and shortened the electron migration distance and time.

Nickel sulfides are another group of popular HER co-catalyst, and have many different compositions and phases. Among them, NiS and NiS_2 have been demonstrated as highly active co-catalyst for photocatalytic H_2produciton.[176-182] Xu *et al.* have shown that the NiS-CdS heterostructures could exhibit a high apparent quantum yield (AQY) of 51.3 % for H_2 production at 420 nm excitation.[176] It was proposed that the proton can bind with Ni^{2+} on NiS surfaces, which facilitates its reduction and consequent H_2 evolution.[183] Similarly, the deposition of NiS_2 nanoparticles onto $CdLa_2S_4$ surfaces also resulted in remarkable enhancement in H_2 generation under visible light irradiation as compared to pristine $CdLa_2S_4$.[181] Both NiS and NiS_2 have been successfully loaded on g-C_3N_4 surfaces to enhance photocatalytic H_2 production.[178, 182]

In comparison to MoS_2 and nickel sulfide, CuS can also act as a co-catalyst but with a different mechanism. Gong *et al.* have prepared CuS-loaded ZnS porous nanosheets via a hydrothermal process with cation exchange.[184] Although ZnS alone is a wide bandgap semiconductor with no visible light activity and CuS alone is also not capable for photocatalytic H_2 generation, CuS-ZnS heterojunctions exhibit high visible-light activity for H_2 production with an AQY of 20% at 420 nm. The authors propose that the interfacial charge transfer (IFCT) from the valence band of ZnS to CuS (Fig. 9) with transition energy of 2.94 eV is responsible for its visible light activity, leading to reduction of surface CuS clusters to Cu_2S as an intermediate product that is subsequently converted back to CuS with accompanied proton reduction into H_2. Following this work, CuS has been also decorated onto other semiconductors including ZnO,[185] CdS,[186] and $Zn_xCd_{1-x}S$,[144,145] to achieve enhanced H_2 production without aids of noble-metals.

It is noteworthy that these metal sulfide co-catalysts, such as MoS_2 and NiS,[102, 126, 187] have also been reported as a type of semiconductor for some photocatalytic reactions. The exact principle of how these metal sulphide co-catalyst function as an electron receptor is still under debate.

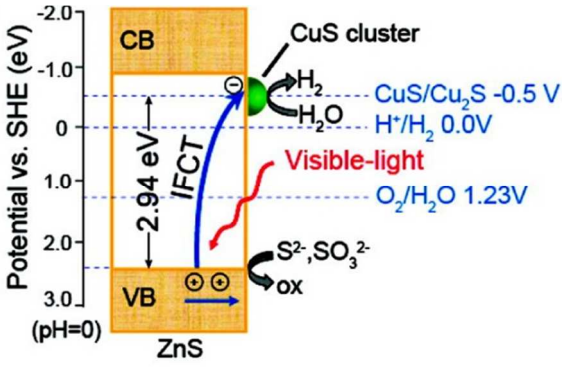

Fig.9 Schematic illustration for the proposed mechanism of visible light induced interfacial charge transfer (IFCT) from the valence band of ZnS to the CuS clusters. Reprinted with permission from Ref. 184. Copyright 2011 American Chemical Society

3.3 Heterojunctions of semiconductor and metal complex

In recent years, some transition metal complexes, such as hydrogenases,[188, 189] hydrogenase mimics,[190, 191] and Ni-complexes,[192, 193] have been proven as active HER co-catalysts when coupled with semiconductor photocatalysts. Unlike metal oxide or sulphide co-catalysts which are deposited onto the semiconductor with intimate contact, these molecular co-catalysts are normally chemisorbed or electrostatically binded on the semiconductor surface. Nevertheless, these interactions still enable the electron transfer from photoexcited semiconductors to the molecular co-catalysts for proton reduction.

For example, by coupling a hydrogenase system consisting of Clostridium acetobutylicum [Fe-Fe]-hydrogenase I (CaI) and CdTe or CdS nanoparticles, high quantum efficiencies of 9% at 523 nm and 20% at 405 nm could be achieved.[188, 189] This is attributed to the fast electron transfer from excited CdTe or CdS to CaI serving as active sites for proton reduction to H_2. Besides natural hydrogenases, artificial hydrogenase mimics, such as dinulear [Fe-Fe]-H_2ase and cobaloximes, have also been used to promote H_2 production through similar electron transfer process.[190, 191, 194, 195]

Recently Krauss *et al.* reported a durable and active system containing dihydrolipoic acid (DHLA) capped CdSe quantum dots as photocatalyst and water soluble Ni^{2+}-DHLA as co-catalyst for H_2 production,[192] which exhibited excellent long-term stability for H_2 production with maintained high quantum yield over 15 days. Although the details of the catalytically active nickel species are still not clear, it was believed that the nickel-thiolate moieties attaching on CdSe surfaces are responsible for proton reduction in this system. Similarly, some other Ni^{2+} complexes, such as $Ni(dmgh)_2$,[196] and $[Ni(TEOA)_2]^{2+}$,[193] have also been reported as effective molecular co-catalyst to couple with semiconductor photocatalysts for efficient H_2 production.

4. Metal-semiconductor heterojunctions for H_2 production and CO_2 reduction

4.1 Schottky junction

The intimate contact of a metal with an n-type semiconductor normally creates a Schottky junction with a potential barrier that prevents most electrons/holes from passing through them. The opposite case of a p-type semiconductor/metal junction represents an ohmic contact. Fig. 10 illustrates the energy band diagram of a typical metal-semiconductor Schottky junction. The height of the potential barrier (Φ_b) depends on the band bending of the semiconductor and the Fermi level of metal at the equilibrium.[197] Upon excitation of the semiconductor, the photogenerated electrons are able to transfer across the Schottky junction to the contacting metal, resulting in a shift of Fermi level of the metal towards that of the semiconductor with a new equilibrium (Fig. 10).[198-200] In this way, the metal acts like an electron sink to enable the separation of photogenerated electrons and holes and thus allowing more time for the holes on the semiconductor surface for oxidation reaction. Furthermore, the metal surface may provide active sites to lower the overpotentials for H_2 generation and CO_2 photoreduction.[170, 201]

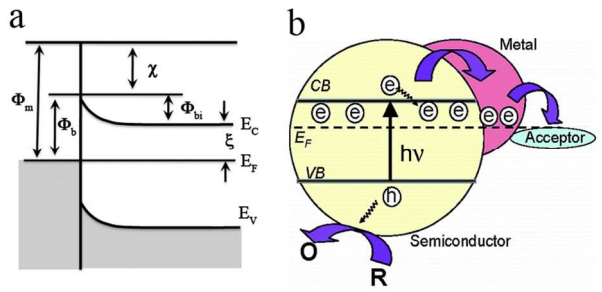

Fig. 10 Schematic illustrations of (a)Schottky junction with energy level alignment and (b) photoinduced electron transfer across the metal-semiconductor junction. Reprinted with permission from ref. 197 and 199. Copyright 2008 and 2004 American Chemical Society.

To achieve efficient electron transfer across the Schottky junction, the Fermi level of the metal should be sufficiently lower than the semiconductor CB. Therefore, metals with large working function (normally larger than 5.0 eV) such as Pt,[136, 202] Pd,[203] Au,[204, 205] Rh,[206] and Ru,[207] have been commonly used to form heterojunctions with semiconductors. In addition, particularly for H_2 generation, the M-H (M as transition metal) bond strength is also a critical issue. The stronger M-H bond may allow for lower activation energy of proton reduction ($H^+ + e^- \rightarrow H_{ad}$), but H_2 desorption ($2H_{ad} \rightarrow H_2$) on the metal surface would be more difficult.[208] Therefore, one has to find a balance on the M-H bond strength for efficient H_2 evolution. Among all metals, Pt has been recognized as the optimal choice in terms of work function and bond strength with hydrogen,[170, 201] and thus is the most popular metal co-catalyst for photocatalyticH_2production.

For example, a simple tip-loading of Pt on CdSe@CdS nanorod could result in an AQY of 20% at 420 nm irradiation for H_2 production.[178] An even higher AQY (60.3%) was reported by Bao *et al.* over porous CdS nanostructures with homogenous loading of Pt nanoparticles via UV-photodeposition, which benefits from the large surface area.[177] Note that the pH of the precursor (e.g. H_2PtCl_6) solution for photodeposition of Pt may also influence the photocatalytic activity of Pt-semiconductor structures. Xu *et al.* found that Pt^{4+} species (in H_2PtCl_6) can be readily reduced to Pt^0 in alkaline solution, while in acidic condition, some Pt^{4+} can only be partially reduced to Pt^{2+}.[209] Thus the CdS particles with Pt-loading at pH 13.5 showed much higher photocatalytic H_2 generation rate than that with Pt loading at pH 2.4.

Due to the high cost of Pt, researchers have attempted to reduce its usage by alloying Pt with earth abundant transition metals with retained high efficiency for H_2 evolution. Yu *et al.* found that loading 1 wt% Pt_3Co onto CdS resulted in about two times higher H_2 production rate than 1 wt% Pt-loaded CdS,[210] which is ascribed to the more effective accumulation of photoexcited electrons on Co than on Pt. Indeed, previous reports also showed that some earth abundant coinage metals, such as Ni,[211-213] Co,[214] Cu,[215, 216] could also act as co-catalysts for H_2 evolution. For instance, Do *et al.* demonstrated that the visible-light-driven H_2 production rate over 1.2 wt% Ni loaded CdS is nearly twice higher than that of 1.2 wt% Pt loaded CdS.[213] Moreover, the nanocomposite of CdS nanoparticles growing on titanate nanodisks exhibited very weak photoactivity for H_2evolution (0.142 mmol g^{-1} h^{-1}) in ethanol-water solution due to the high overpotential on titanate surfaces. However, loading of nickel clusters onto this composite led to 80 times enhancement on the photocatalytic H_2 generation rate because the Ni clusters on titanate surfaces can trap the electrons injected from excited CdS and act as active sites for H_2 evolution.

Besides H_2 evolution, the metal-semiconductor Schottky junction can also be used for enhanced CO_2photoreduction, and the loaded metal may exhibit certain selectivity for hydrocarbon formation. For example, CO_2 photoreduction over Pd-loaded TiO_2 led to CH_4 as the main product and minor production of C_2H_6 and CO.[217] Wang *et al.* demonstrated that the film of 1-D single crystal TiO_2 coated with ultrafine Pt nanoparticles (0.5-2 nm) exhibited very high efficiency of CO_2 photoreduction with selective formation of methane (1361 μmol/g-cat/h).[218]

Previous studies also proved that Cu could act as active co-catalyst for CO_2 photoduction.[219, 220] In 2010, Biswas *et al.* prepared mesoporous silica supported Cu-TiO_2 nanocomposites for efficient CO_2 photoreduction.[221] Without Cu co-catalyst, CO was found to be the main product, while the Cu-loading on TiO_2led to higher selectivity in CO_2 reduction into CH_4. The same group subsequently reported the rapid preparation of Cu-TiO_2-SiO_2 hybrids by evaporation driven self-assembly of nanocolloids for high yield photo-conversion of CO_2 into CO.[222]

4.2 Plasmonic metal-semiconductor heterojunctions

In the past decade, the nanostructures of some noble metals such as Au, Ag and Pd, have attracted particularly strong interest due to their interactions with visible-light induced by surface plasmon resonance (SPR), referring to the collective coherent oscillations of metal surface electrons against the restoring force of positive nuclei.[223, 224] The SPR wavelengths highly depend on the composition, size, shape, geometric arrangement, and dielectric environment of the plasmonic metal nanostructures.[225] This strong SPR effect has been used to improve the light-harvesting capability in photovoltaic devices due to light-trapping by the localized oscillating electric field of metal nanostructures. [226]

In 2005, Tatsuma *et al.* reported the first direct observation of plasmon-induced photocurrent on the TiO_2 film loaded with Au nanoparticles, and the action spectra for IPCE matched well with the absorption band of the Au particles.[227] Later, the plasmon-induced photocurrent was also observed by other groups over different metal oxide-Au heterojunctions.[83, 228, 229] By using ultrafast spectroscopy, Furube *et al.* have proven that upon plasmon excitation, the hot electrons of Au particles can be inject into TiO_2 conduction band within 250 fs,[230] and these electrons are capable of diffusing into TiO_2 for 100 ps~10 ns depending on the particle size,[231] leading to plasmon-induced charge separation. Brückner *et al.* further proved the plasmon-driven electron transfer from Au particles to TiO_2 by electron paramagnetic resonance (EPR) spectroscopy, and found that the injected hot electrons are trapped in the vacancies near the Au-TiO_2interface.[232] These observations imply that the hot-plasmon electrons can be used for some chemical reactions such as proton reduction to H_2 under visible-light irradiation.

For instance, García *et al.* have observed clear H_2 production over Au-TiO_2 composites under irradiation at 532 nm.[233] Other researchers further reported that the crystal facet and superstructure of TiO_2 have significant effect on the H_2 generation activity because it influences the transport ability of

injected hot electrons to the active site for proton reduction.[234, 235] Nevertheless, the activity of plasmon-induced H_2 evolution over Au-TiO_2 heterojunctions is still very low because the TiO_2 surfaces have high overpotential for H_2 evolution. To solve this issue, Kiminami *et al.* demonstrated that the co-loading of other metal co-catalysts onto Au-TiO_2 structures led to improved H_2 generation rate upon Au SPR excitation.[236] Moreover, through systematic studies with dual-beam irradiation over the Au/Pt co-decorated TiO_2 nanofibers, Zhang *et al.* found a synergistic effect between Au SPR and TiO_2 excitation, and indicated that the plasmon-driven H_2 generation can be significantly enhanced when the TiO_2 is co-excited (Fig. 11). This might enhance TiO_2 conductivity so that the injected hot electrons from Au can be more effectively transported through TiO_2 to nearby Pt sites for H_2 evolution.[237]

In addition to TiO_2, some other materials have also been used to form heterojunctions with Au nanoparticles to observe plasmon-induced H_2 evolution. For instance, Halas *et al.* have demonstrated hot-electron-induced photodissociation of H_2 on small Au nanoparticles supported on SiO_2.[238] Interestingly, a recent study by Zheng *et al.* showed that even a bimetallic nanostructure, Au nanorod with tip-loading of Pt, can exhibit H_2 evolution in methanol through plasmon-induced hot electron transfer from Au to Pt.[239] Similar process was also observed over the Pt/Au/WO_3 photocatalysts with H_2 generation in the presence of glycerin or 2-propanol.[240] However, as more Pt are deposited onto gold particle surface, the Au SPR would be gradually dampened, leading to a decrease in the plasmon-driven photocatalytic activity.[241]

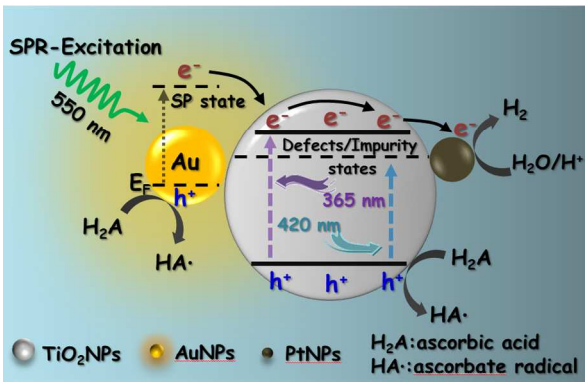

Fig. 11 Plasmon-driven photocatalytic hydrogen production over Au/Pt-TiO_2 nanofibers. The hot plasmon electrons of Au nanoparticles can readily transport through TiO_2 (when it is co-excited) to the nearby Pt particle for hydrogen generation. Reprinted from ref. 237 with permission from The Royal Society of Chemistry.

Besides the hot-electron mechanism, the plasmon-enhanced localized electric field has also been considered as another major contribution to the improved photocatalytic activity over plasmonic metal-semiconductor hybrid nanostructures. Upon SPR excitation, the local electric field nearby the metal particle surfaces can be significantly enhanced, and the enhancement factor drops exponentially along with the distance from the metal surface.[223] Hence, the semiconductor that is located very near the metal surface would be exposed to this strong plasmonic field which can enhance the semiconductor excitation with more exciton formation,[242-244] leading to higher photocatalytic efficiency.

For example, Kumar *et al.* prepared a plasmonic $TiO_2/SiO_2/Ag$ system in which the TiO_2 film was deposited onto the Ag nanoparticle film with a very thin or SiO_2 spacers between TiO_2 and Ag for the purpose of excluding injection of hot plasmon electrons. This tri-layer structure still showed enhanced photocatalytic activity with higher enhancement at smaller SiO_2 layer thickness, which proves the effect of this plasmon field-enhancement mechanism.[243] Han *et al.* Have reported an interesting Janus Au-TiO_2 nanoparticles that exhibit enhanced H_2 generation in isopropanol solution under visible-light irradiation with the rate of hydrogen generation following the order of Au_{70nm}-TiO_2>Au_{50nm}-TiO_2>Au_{30nm}-TiO_2.[245] The authors attributed the higher H_2 generation rate to the strong Au plasmonic near field that enhanced the optical absorption and of electron-hole pair generation on the conjugated TiO_2 particle.

Besides the near-field enhancement, the SPR effect of metal nanoparticles can also promote the charge separation of nearby semiconductor through a process of plasmon-induced resonance energy transfer (PIRET), in which the plasmonic energy is transferred from metal to semiconductor through dipole-dipole interaction to induce charge separation in the semiconductor. [246] Importantly, the PIRET process enables the generation of charge carriers even if the excitation photon energy is below the band gap, and thereby allows us to utilize wide ranges of low energy photons for photocatalytic reactions.

In addition to H_2 production, plasmonic metal-semiconductor nanostructures have also been utilized for CO_2 photoreduction. Cronin *et al.* have achieved 24-fold enhancement in CO_2 reduction over Au-TiO_2 heterojunctions when the incident photon energy matches the SPR of gold nanoparticles.[247] Enhanced CO_2 photoconversion to CH_4 has also been reported by Fan *et al.*by using Ag-loaded TiO_2 nanocomposites.[248] Recently, Zhang *et al.* showed that co-loading of gold nanoparticles into the Pt-TiO_2 nanofibers can result in higher efficiency for CO_2 photoreduction due to plasmon field enhancement.

4.3 Z-scheme heterostructure of Semiconductor-metal-semiconductor

The concept of Z-scheme was originated from the natural leaf that utilizes two red photons to accomplish the photosynthetic processes. As shown in Fig. 12, the biomimetic Z-scheme water splitting system consisting of two isolated semiconductors and redox couples in liquid electrolytes.[249] However, the overall working efficiency in this Z-scheme is restricted by the slow diffusion of redox couple ions and the competitive backward reactions between them. In order to avoid these drawbacks, researchers have proposed "all-solid-state" Z-scheme by using noble metal as the electron mediator to substitute solution-based redox couples, resulting in a ternary heterostructure of semiconductor-metal-semiconductor.[84,85] Though some examples of Z-scheme semiconductor-metal-semiconductor heterostructure have been demonstrated with successful outcomes for photocatalytic water splitting or CO_2 reduction,[250, 251] currently there is still a lack of solid evidence to verify the proposed Z-scheme electron transfer path.

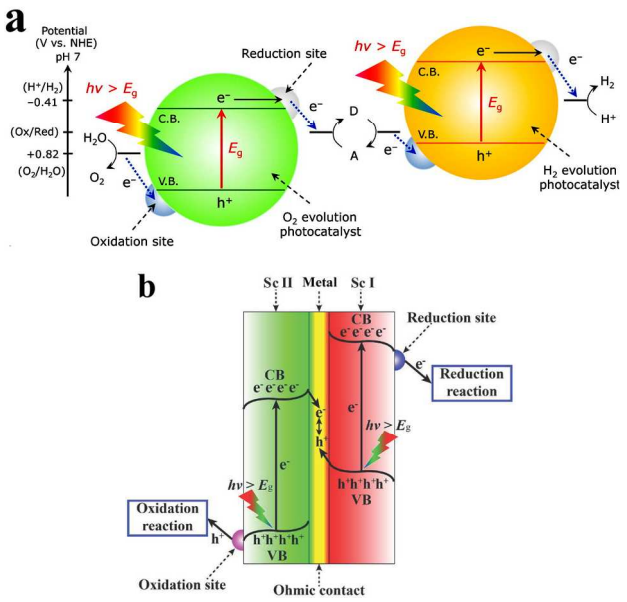

Fig.12 Schematic illustration of (a) liquid-based Z-scheme for water splitting; (b) "all-solid-state" Z-scheme consisting of semiconductor I (Sc I)-metal-semiconductor II (Sc II). Reprinted with permission from ref. 249 and 251. Copyright 2013 American Chemical Society (a) and 2014 Wiley (b).

5. Conclusion and perspectives

Significant advances have been achieved in designing and fabricating hetero-nanostructure photocatalysts for efficient photocatalytic H_2 production and CO_2 reduction in the past decade. Although the photocatalytic activities, in most cases, can be enhanced by creating appropriate heterojunctions, actual solar-to-fuel conversion efficiencies are still a far cry from meeting the criteria for commercialization. This is due to the limitations of semiconductor photocatalysts such as high overpotentials for H_2/O_2 evolution and its very low activity for red-photons or near-IR light. In particular, long-term stability is the most serious problem especially for those noble-metal-free structures. Beside these, there are still several important issues to be addressed in design and fabrication of heterostructured photocatalysts in the future to achieve satisfying efficiency in solar-to-fuel conversion.

I: Charge transfer/separation at the interface: Though there is general consensus that heterojunctions facilitate migration of photoexcited electrons or/and holes across the interfaces so as to reduce charge recombination or enhance charge separation, there were very few direct experimental evidences or spectroscopic observations that unambiguously reveal the detailed mechanism of the photoinduced charge transfer process at the interface of heterostructures. The key challenges come from the interference between multiple complicated variables, such as surface status (crystal facets, defects, trapping sites etc.), excitation/relaxation dynamics, and surface reaction kinetics, especially when two or more components in the heterostructure are making contributions simultaneously during the studies. Nevertheless, it is still important and critical to gain deep understanding on the charge transfer process through fundamental studies towards rational design of heterostructures with high photocatalytic efficiencies.

II: Competitive light-harvesting: The semiconductor-based photocatalysts are mostly active in the spectral region with high-energy photons (e.g. UV or blue light). Although some of them do exhibit certain visible-light activity, their photo-conversion efficiency is very low. This problem becomes more notable for semiconductor heterostructures because the two semiconductor components would have to compete in absorbing high-energy photons for charge carrier generation, especially if their absorption range has a large overlap. Therefore, it is challenging to design heterostructures with the appropriate morphological-related orientation and position of each semiconductor unit within the structure. Alternatively, one would need to develop a new type of semiconductor that can efficiently utilize red photons or near-IR light with suitable band structure and high stability.

III: Interfaces versus surfaces: For heterostructures, the interface area is often critical to achieve optimal charge separation. Especially for heterojunctions between two semiconductors, whereby a larger interface area would provide more chances for charge transfer across the junction towards a more efficient separation of photogenerated electrons and holes on both units. Based on this concern, it is important to have nanoscale units to create the heterojunction, allowing for large interface area and reduced charge transport length towards the heterojunction. However, the overall photocatalytic efficiency is determined not only by charge separation, but also surface reactions. Thus in the preparation of heterostructures, there would be strong challenges on how to balance the interfaces with the available surface area for redox reactions. More importantly, more systematic studies are required to explore theories or experimental methods to determine or estimate the optimal ratio between interface and bare surface in different heterostructures.

Acknowledgements

The authors would like to thank the financial support from NTU seed funding for the Solar Fuels Laboratory, MOE AcRF-Tier1 RG 44/11, MOE AcRF-Tier2 (MOE2012-T2-2-041, ARC 5/13), and CRP (NRF-CRP5-2009-04) from NRF Singapore. Y. P. Yuan thanks the financial support from the National Natural Science Foundation of China (No. 51002001, 21303002), and acknowledges the group members, Lingli Liu, Haiyu Chen and Xin Jiang for their assistance in preparing the materials.

Notes and references

[a]*Laboratory of Advanced Porous Materials, School of Chemistry and Chemical Engineering, Anhui University, Hefei 230601, P. R. China.*
[b]*Department of Life Sciences, Imperial College London, South Kensington Campus London SW7 2AZ, U.K.*
[c]*Solar Fuels Lab, School of Materials Science and Engineering, Nanyang Technological University, 50 Nanyang Avenue, Singapore 639798, Singapore; E-mail: joachimloo@ntu.edu.sg; cxue@ntu.edu.sg*

References

1. http://cdiac.ornl.gov/GCP/carbonbudget/2013/
2. N. S. Lewis and D. G. Nocera, *Proc. Natl Acad. Sci. USA*, 2006, **103**, 15729-15735.
3. S. N. Habisreutinger, L. Schmidt-Mende and J. K. Stolarczyk, *Angew.Chem. Int. Ed.*,2013, **52**, 7372-7408.

4.Y. Yuan, Z. Zhao, J. Zheng, M. Yang, L. Qiu, Z. Li and Z. Zou, *J.Mater. Chem.*, 2010, **20**, 6772-6779.

5.F. E. Osterloh, *Chem. Mater.*, 2008, **20**, 35-54.

6.A. Kudo and Y. Miseki, *Chem. Soc. Rev.*, 2009, **38**, 253-278.

7.X. B. Chen, S. H. Shen, L. J. Guo and S. S. Mao, *Chem. Rev.*, 2010, **110**, 6503-6570.

8.H. Tong, S. Ouyang, Y. Bi, N. Umezawa, M. Oshikiri and J. Ye, *Adv. Mater.*, 2012, **24**, 229-251.

9.K. Maeda and K. Domen, *J. Phys. Chem. Lett.*, 2010, **1**, 2655-2661.

10.R. Asahi, T. Morikawa, T. Ohwaki, K. Aoki and Y. Taga, *Science*, 2001, **293**, 269-271.

11.S. U. M. Khan, M. Al-Shahry and W. B. I. Jr., *Science*, 2002, **297**, 2243-2245.

12. X. B. Chen, C. Li, M. Gratzel, R. Kostecki and S. S. Mao, *Chem. Soc. Rev.*, 2012, **41**, 7909-7937.

13.D. V. Bavykin, V. N. Parmon, A. A. Lapkin and F. C. Walsh, *J. Mater. Chem.*, 2004, **14**, 3370-3377.

14.M. T. Mayer, Y. Lin, G. Yuan and D. Wang, *Acc. Chem. Res.*, 2013, **46**, 1558-1566.

15.J. S. Jang, H. G. Kim and J. S. Lee, *Catal.Today*, 2012, **185**, 270-277.

16.W. Q. Fan, Q. H. Zhang and Y. Wang, *Phys. Chem. Chem. Phys.*, 2013, **15**, 2632-2649.

17.Y. J. Wang, Q. S. Wang, X. Y. Zhan, F. M. Wang, M. Safdar and J. He, *Nanoscale*, 2013, **5**, 8326-8339.

18.K. S. Joya, Y. F. Joya, K. Ocakoglu and R. van de Krol, *Angew. Chem. Int. Ed.*, 2013, **52**, 10426-10437.

19.Z. S. Li, W. J. Luo, M. L. Zhang, J. Y. Feng and Z. G. Zou, *Energy Environ. Sci.*, 2013, **6**, 347-370.

20.Y. Park, K. J. McDonaldb and K. S. Choi, *Chem. Soc. Rev.*, 2013, **42**, 2321-2337.

21.L. Li, P. A. Salvador and G. S. Rohrer, *Nanoscale*, 2014, **6**, 24-42.

22.H. T. Yu and X. Quan, *Prog. Chem.*, 2009, **21**, 406-419.

23.Y. Bessekhouad, D. Robert and J. V. Weber, *Catal. Today*, 2005, **101**, 315-321.

24.Y. Bessekhouad, D. Robert and J. V. Weber, *J. Photochem. Photobiol., A*, 2004, **163**, 569-580.

25.A. Mills and S. L. Hunte, *J. Photochem. Photobiol., A*, 1997, **108**, 1-35.

26. A. L. Linsebigler, G. Q. Lu, J. T. Yates and Jr., *Chem. Rev.*, 1995, **95**, 735-758.

27.M. R. Hoffmann, S. T. Martin, W. Choi and D. W. Bahnemannt, *Chem. Rev.*, 1995, **95**, 69-96.

28.X. B Chen and S. S. Mao,*Chem. Rev.*, 2007, **107**, 2891-2959.

29.M. D. Hernández-Alonso, F. Fresno, S. Suárez and J. M. Coronado, *Energy Environ. Sci.*, 2009, **2**, 1231-1257.

30. D. C. Hurum, A. G. Agrios, K. A. Gray,T. Rajh and M. C. Thurnauer, *J. Phys. Chem. B*, 2003, **107**, 4545-4549.

31. B. Sun, A. V. Vorontsov and P. G. Smirniotis, *Langmuir*, 2003, **19**, 3151-3156.

32. Q. Xu, Y. Ma, J. Zhang, X. L. Wang, Z. C. Feng and C. Li, *J. Catal.*, 2011, **278**, 329-335.

33.L. Kavan, M. Gra1tzel, S. E. Gilbert, C. Klemenz and H. J. Scheel, *J. Am. Chem. Soc.*, 1996, **118**, 6716-6723.

34.D. O. Scanlon, C. W. Dunnill, J. Buckeridge, S. A. Shevlin, A. J. Logsdail1, S. M.Woodley, C. R. A. Catlow, M. J. Powell, R. G. Palgrave, I. P. Parkin, G. W. Watson, T. W. Keal, P. Sherwood, A. Walsh and A. A. Sokol1, *Nat. Mater.*, 2013, **12**, 798-801.

35. T. Ohno, T. Higo, N. Murakami, H. Saito, Q. T. Zhang, Y. Yang and T. Tsubota, *Appl. Catal., B,*2014, **152-153**, 309-316.

36.T. A. Kandiel, A. Feldhoff, L. Robben, R. Dillert and D. W.Bahnemann, *Chem. Mater.*, 2010, **22**, 2050-2060.

37.X. J. Shen, J. L. Zhang, B. Z. Tian and M. Anpo, *J. Mater. Sci.*, 2012, **47**, 5743-5751.

38.H. Xu and L. Z. Zhang, *J. Phys. Chem. C*, 2009, **113**, 1785-1790.

39.R. Boppella, P. Basak and S. V. Manorama, *ACS Appl. Mater. Interfaces*, 2012, **4**, 1239-1246.

40.Q. Tay, X. F. Liu, Y. X. Tang, Z. L. Jiang, T. C. Sum and Z. Chen, *J. Phys. Chem. C*, 2013, **117**, 14973-14982.

41. Y. X. Liu, Z. L. Wang, W. D. Wang and W. X. Huang, *J. Catal.*, 2014, **310**, 16-23.

42. X. Wang, Q. Xu, M. R. Li, S. Shen, X. L. Wang, Y. C. Wang, Z. C. Feng, J. Y. Shi, H. X. Han and C. Li, *Angew. Chem. Int. Ed.*, 2012, **51**, 13089-13092.

43. P. Wang, P. R. Chen, A. Kostka, R. Marschall and M. Wark, *Chem. Mater.*, 2013, **25**, 4739-4745.

44. M. C. Liu, D. W. Jing, Z. H. Zhou and L. J. Guo, *Nat. Commun.*, 2013, **4**, 2278.

45. David O. Scanlon and G. W. Watson, *J. Phys. Chem. Lett.*, 2010, **1**, 2582-2585.

46. T. F. Jiang, T. F. Xie, W. S. Yang, L. P. Chen, H. M. Fan and D. J. Wang, *J. Phys. Chem. C*, 2013, **117**, 4619-4624.

47. L. C.K. Liau, Y.C. Lin and Y.J. Peng, *J. Phys. Chem. C*, 2013, **117**, 26426-26431.

48. M. K. Nowotny, P. Bogdanoff, T. Dittrich, S. Fiechter, A. Fujishima and H. Tributsch, *Mater. Lett.*, 2010, **64**, 928-930.

49. A. R. Ballyyz, E. N. Korobeinikovax, P. E. Schmid and F. Bussyk, *J. Phys. D: Appl. Phys.*, 1998, **31**, 1149–1154.

50. J. Chen, P. Rulis, L. Z. Ouyang, S. Satpathy and W. Y. Ching, *Phys. Rev. B*, 2006, **74**, 235207.

51. C. Kim, K.S. Kim, H. Y. Kim and Y. S. Han, *J. Mater. Chem.*, 2008, **18**, 5809-5814.

52. A. Ruiz, A. Cornet, G. Sakai, K. Shimanoe, J. R. Morante and N. Yamazoe, *Chem. Lett.*, 2002, **31**, 892-893.

53. S. Liu, T. H. Xie, Z. Chen and J. T. Wu, *Appl. Surf. Sci*, 2009, **255**, 8587-8592.

54. S. F. Chen, X. L. Yu, H. Y. Zhang and W. Liu, *J. Electrochem. Soc.* , 2010, **157**, K96-K102.

55. J. Zhang, X. H. Tang and D. Y. Li, *J. Phys. Chem. C*, 2011, **115**, 21529-21534.

56. J.P. Zou, S.L. Lei, J. Yu, S.L. Luo, X.B. Luo, X.H. Tang, W.L. Dai, J. Sun, G.C. Guo and C.T. Au, *Appl. Catal., B*, 2014, **150-151**, 466-471.

57. H. Zhou, L. Ding, T. X. Fan, J. Ding, D. Zhang and Q. X. Guo, *Appl. Catal., B*, 2014, **147**, 221-228.

58. J. S. Jang, H. G. Kim, U. A. Joshi, J. W. Jang and J. S. Lee, *Int. J. Hydrogen Energy* 2008, **33**, 5975-5980.

59. H. Park, W. Choi and M. R. Hoffmann, *J. Mater. Chem.*, 2008, **18**, 2379-2385.

60. S. Banerjee, S. K. Mohapatra and M. Misra, *J. Phys. Chem. C*, 2011, **115**, 12643-12649.

61. S. Xu and D. D. Sun, *Int. J. Hydrogen Energy* 2009, **34**, 6096-6104.

62. Z. L. Wang, Y. X. Liu, D. J. Martin, W. D. Wang, J. W. Tang and W. X. Huang, *Phys. Chem. Chem. Phys.*, 2013, **15**, 14956-14960.
63. B. Chai, T. Y. Peng, P. Zeng and J. Mao, *J. Mater. Chem.*, 2011, **21**, 14587-14593.
64. C. J. Wang, R. L. Thompson,J. Baltrus and C. Matranga, *J. Phys. Chem. Lett.*, 2010, **1**, 48-53.
65. M. A. Asi, C. He, M. H. Su, D. H. Xia, L. Lin, H. Q. Deng, Y. Xiong, R. L. Qiu and X. Z. Li, *Catal. Today*, 2011, **175**, 256-263.
66. C. J. Wang, R. L. Thompson, P. Ohodnicki, J. Baltrus and C. Matranga, *J. Mater.Chem.*, 2011, **21**, 13452-13457.
67. D. R. Baker and P. V. Kamat, *Adv. Funct. Mater.*, 2009, **19**, 805-811.
68. J. C. Kim, J. Choi, Y. B. Lee, J. H. Hong, J. I. Lee, J. W. Yang, W. I.Lee and N. H. Hur, *Chem. Commun.*, 2006, 5024-5026.
69. H. Y. Wang, W. Zhu, B. H. Chong and K. Qin, *Int. J. Hydrogen Energy*,2014, **39**, 90-99.
70. L. P. Wu, J. Li, S. H. Zhang, L. Z. Long, X. J. Li and C. P. Cen, *J. Phys. Chem. C*, 2013, **117**, 22591-22597.
71. S. S. Kalanur, S. H. Lee, Y. J. Hwang and O.S. Joo, *J. Photochem. Photobiol., A*, 2013, **259**, 1-9.
72. C. L. Li, J. Yuan, B. Y. Han, L. Jiang and W. F. Shangguan, *Int. J. Hydrogen Energy*,2010, **35**, 7073-7079.
73. J. Bai, J. H. Li, Y. B. Liu, B. X. Zhou and W. M. Cai, *Appl. Catal., B*,2010, **95**, 408-413.
74. F. L. Su, J. W. Lu, Y. Tian, X. B. Ma and J. L. Gong, *Phys. Chem. Chem. Phys.*, 2013, **15**, 12026-12032.
75. X. F. Cui, G. Y. Jiang, M. Zhu, Z. Zhao, L. C. Du, Y. X. Weng, C. M. Xu, D. K. Zhang, Q. L. Zhang, Y. C. Wei, A. J. Duan, J. Liu and J. S. Gao, *Int. J. Hydrogen Energy*,2013, **38**, 9065-9073.
76. G. S. Wu, M. Tian and A. C. Chen, *J. Photochem. Photobiol., A*,2012,**233**, 65-71.
77. S. Chaguetmi, F. Mammeri, M. Pasut, S. Nowak, H. Lecoq, P. Decorse, C. Costentin, S. Achour and S. Ammar, *J. Nanopart. Res.*, 2013, **15**, 2140.
78. H. N. Kim, T. W. Kim, I. Y. Kim and S.J. Hwang, *Adv. Funct. Mater.*, 2011, **21**, 3111-3118.
79. W. T. Sun, Y. Yuan, H. Y. Pan, X. F. Gao, Q. Chen, and L.M. Peng, *J. Am. Chem. Soc.*, 2008, **130**, 1124-1125.
80. S. Pang, K. Cheng, Z. Q. Yuan, S. Y. Xu, G. Cheng and Z. L. Du, *Appl. Phys. Lett.*, 2014, **104**, 201601.
81. H. Wang, Y. S. Bai, H. Zhang, Z. H. Zhang, J. H. Li and L. Guo, *J. Phys. Chem. C*, 2010, **114**, 16451-16455.
82. P. V. Kamat, K. Tvrdy, D.R. Baker and J. G. Radich, *Chem. Rev.*, 2010, **110**, 6664-6688.
83. J. Li, S. K. Cushing, P. Zheng, T. Senty, F. Meng, A. D. Bristow, A. Manivannan and N. Wu, *J. Am. Chem. Soc.*, 2014, **136**, 8438-8449.
84. H. Tada, T. Mitsui, T. Kiyonaga, T. Akita and K. Tanaka, *Nat. Mater.*, 2006, **5**, 782-786.
85. H. J. Yun, H. Lee,N. D. Kim, D. M. Lee, S. Yu and J. Yi, *ACS Nano*, 2011, **5**, 4084-4090.
86. J. Fang, L. Xu, Z. Zhang, Y. Yuan, S. Cao, Z. Wang, L. Yin, Y. Liao and C. Xue, *ACS Appl. Mater. Interfaces*, 2013, **5**, 8088-8092.
87. Z. B. Yu, Y. P. Xie, G. Liu, G. Q. Lu, X. L. Ma and H.M. Cheng, *J. Mater. Chem. A*, 2013, **1**, 2772-2776.
88. L. Ding, H. Zhou, S. Lou, J. Ding, D. Zhang, H. X. Zhu and T. X. Fan, *Int. J. Hydrogen Energy*,2013, **38**, 8244-8253.
89. S. Cho, J.W. Jang, S.H. Lim, H. J. Kang, S.W. Rhee, J. S. Lee and K.H. Lee, *J. Mater. Chem.*, 2011, **21**, 17816-17822.
90. X. X. Zou, P. P. Wang, C. G. Li, J. Zhao, D. J. Wang, T. Asefa and G. D. Li, *J. Mater. Chem. A*, 2014, **2**, 4682-4689.
91. X. W. Wang, G. Liu, Z. G. Chen, F. Li, L. Z. Wang, G. Q. Lu and H.M. Cheng, *Chem. Commun.*, 2009, 3452-3454.
92. Z. Wang, S.W. Cao, S. C. J. Loo and C. Xue, *CrystEngComm*, 2013, **15**, 5688-5693.
93. A. Kargar, Y. Jing, S. J. Kim, C. T. Riley,X. Q. Pan and D. L. Wang, *ACS Nano*, 2013, **7**, 11112-11120.
94. Y. B. Li, Z. F. Liu, Y. Wang, Z. C. Liu, J. H. Han and J. Ya, *Int. J. Hydrogen Energy*, 2012, **37**, 15029-15037.
95. J. Lv, T. Kako, Z. S. Li, Z. G. Zou and J. H. Ye, *J. Phys. Chem. C*, 2010, **114**, 6157-6162.
96. A. Nashim , S. Martha and K. M. Parida, *ChemCatChem*, 2013, **5**, 2352-2359.
97. D. F. Wang, Z. G. Zou and J. H. Ye, *Chem. Mater.*, 2005, **17**, 3255-3261.
98. X. Wang, S. Shen, S. Q. Jin, J. X. Yang, M. R. Li, X. L. Wang, H. X. Han and C. Li, *Phys. Chem. Chem. Phys.*, 2013, **15**, 19380-19386.
99. H. G. Kim, P. H. Borse, W. Choi and J. S. Lee, *Angew. Chem. Int. Ed.*,2005, **44**, 4585-4589.
100. H. G. Kim, P. H. Borse, J. S. Jang, E. D. Jeong, O. S. Jung, Y. J. Suh and J. S. Lee, *Chem. Commun.*, 2009, 5889-5891.
101. E. S. Kim, N. Nishimura, G. Magesh, J. Y. Kim, J. W. Jang, H. Jun, J. Kubota, K. Domen and J. S. Lee, *J. Am. Chem. Soc.*, 2013, **135**, 5375-5383.
102. J. Zhang, S. Z. Qiao, L. F. Qi and J. G. Yu, *Phys. Chem. Chem. Phys.*, 2013, **15**, 12088-12094.
103. I. J. L. Plante, A. Teitelboim, I. Pinkas, D. Oron and T. Mokari, *J. Phys. Chem. Lett.*, 2014, **5**, 590-596.
104. J. Bandara, C. P. Udawatta and C. S. Rajapakse, *Photochem.Photobiol. Sci.*, 2005, **4**, 857-861.
105. S. Xu, J. Ng, X. Zhang, H. Bai and D. D. Sun, *Int. J. Hydrogen Energy*, 2010, **35**, 5254-5261.
106. D. P. Kumar, M. V. Shankar, M. M. Kumari, G. Sadanandam, B. Srinivas and V. Durgakumari, *Chem. Commun.*, 2013, **49**, 9443-9445.
107. K. S. Novoselov, A. K. Geim, S. V. Morozov, D. Jiang, Y. Zhang, S. V. Dubonos, I. V. Grigorieva and A. A. Firsov,*Science*, 2004, **306**, 666-669.
108. A. K. Geim, *Science*, 2009, **324**, 1530-1534.
109. J. S. Lee, K. H. You and C. B. Park, *Adv. Mater.*, 2012, **24**, 1084-1088.
110. J. T. Zhang, Z. G. Xiong and X. S. Zhao, *J. Mater. Chem.*, 2011, **21**, 3634-3640.
111. Y. J. Yu, Y. Zhao, L. E. Brus, K. S. Kim and P. Kim, *Nano Lett.*,2009, **9**, 3430-3434.
112. Q. J. Xiang, J. G. Yu and M. Jaroniec, *Chem. Soc. Rev.*, 2012, **41**, 782-796.
113. X. An and J. C. Yu, *RSC Adv.*, 2011, **1**, 1426-1434.
114. F. Meng, J. Li, S. K. Cushing, J. Bright, M. Zhi, J. D. Rowley, Z. Hong, A. Manivannan, A. D. Bristow and N. Wu, *ACS Catal.*, 2013, **3**, 746-751.
115. K.Y. Lian, Y.F. Ji, X.F. Li, M.X. Jin, D.J. Ding and Y. Luo, *J. Phys. Chem. C*, 2013, **117**, 6049-6054.

116. T.F. Yeh, J.M. Syu, C. Cheng, T.H. Chang and H. Teng, *Adv. Funct. Mater.*, 2010, **20**, 2255-2262.
117. A. Mathkar, D. Tozier, P. Cox, P. Ong, C. Galande, K. Balakrishnan, A. L. M. Reddy and P. M. Ajayan, *J. Phys. Chem. Lett.*, 2012, **3**, 986-991.
118. X.Y. Zhang, H.P. Li, X.L. Cui and Y. Lin, *J. Mater. Chem.*, 2010, **20**, 2801-2806.
119. X. Cao, G. Tian, Y. Chen, J. Zhou, W. Zhou, C. Tian and H. Fu, *J. Mater. Chem. A*,2014, **2**, 4366-4374.
120. Q. J. Xiang, J. G. Yu and M. Jaroniec, *Nanoscale*, 2011, **3**, 3670-3678.
121. Q. Li, B. D. Guo, J. G. Yu, J. R. Ran, B. H. Zhang, H. J. Yan and J. R. Gong, *J. Am. Chem. Soc.*, 2011, **133**, 10878-10884.
122. L. Jia, D.H. Wang, Y.X. Huang, A.W. Xu and H.Q. Yu, *J. Phys. Chem. C*, 2011, **115**, 11466-11473.
123. Q. Li, H. Meng, J. G. Yu, W. Xiao, Y. Q. Zheng and J. Wang, *Chem. Eur. J.*, 2014, **20**, 1176-1185.
124. J. Zhang, W. W. Zhao, Y. Xu, H. L. Xu and B. Zhang, *Int.J. Hydrogen Energy*, 2014, **39**, 702-710.
125. X. W. Wang, L. C. Yin and G. Liu, *Chem. Commun.*, 2014, **50**, 3460-3463.
126. F. Meng, J. Li, S. K. Cushing, M. Zhi and N. Wu, *J. Am. Chem. Soc.*, 2013, **135**, 10286-10289.
127. Y. Chen, H. Ge, L. Wei, Z. Li, R. Yuan, P. Liu and X. Fu, *Catal. Sci. Technol.*, 2013, **3**, 1712-1717.
128. W. G. Tu, Y. Zhou, Q. Liu, S. C. Yan, S. S. Bao, X. Y. Wang, M. Xiao and Z. G. Zou, *Adv. Funct. Mater.*, 2013, **23**, 1743-1749.
129. J. G. Yu, J. Jin, B. Cheng and M. Jaroniec, *J. Mater. Chem. A*, 2014,**2**, 3407-3416.
130. Y. T. Liang, B. K. Vijayan, K. A. Gray and M. C. Hersam, *Nano Lett.*, 2011, **11**, 2865-2870.
131. X. C. Wang, K. Maeda, A. Thomas, K. Takanabe, G. Xin, J. M. Carlsson, K. Domen and M. Antonietti, *Nat.Mater.*, 2009, **8**, 76-80.
132. Y. Zheng, J. Liu, J. Liang, M. Jaroniec and S. Z. Qiao, *Energy Environ. Sci.*, 2012, **5**, 6717-6731.
133. S. C. Yan, Z. S. Li and Z. G. Zou, *Langmuir*, 2009, **25**, 10397-10401.
134. F. Dong, L. W. Wu, Y. J. Sun, M. Fu, Z. B. Wu and S. C. Lee, *J. Mater. Chem.*, 2011, **21**, 15171-15174.
135. J. H. Liu, T. K. Zhang, Z. C. Wang, G. Dawson and W. Chen, *J. Mater. Chem.*, 2011, **21**, 14398-14401.
136. Y.P. Yuan, W.T. Xu, L.S. Yin, S.W. Cao, Y.S. Liao, Y.Q. Tng and C. Xue, *Int. J. Hydrogen Energy*, 2013, **38**, 13159-13163.
137. X.H. Li, X. Wang and M. Antonietti, *Chem. Sci.*, 2012, **3**, 2170-2174.
138. S. B. Yang, Y. J. Gong, J. S. Zhang, L. Zhan, L. L. Ma, Z. Y. Fang, R. Vajtai, X. C. Wang and P. M. Ajayan, *Adv. Mater.*, 2013, **25**, 2452-2456.
139. Y. Zhang, T. Mori, L. Niu and J. Ye, *Energy Environ. Sci.*, 2011, **4**, 4517-4521.
140. G. Liao, S. Chen, X. Quan, H. Yu and H. Zhao, *J. Mater. Chem.*, 2012, **22**, 2721-2726.
141. A. Du, S. Sanvito, Z. Li, D. Wang, Y. Jiao, T. Liao, Q. Sun, Y. H. Ng, Z. Zhu, R. Amal and S. C. Smith, *J. Am. Chem. Soc.*, 2012, **134**, 4393-4397.
142. Q. Xiang, J. Yu and M. Jaroniec, *J. Phys. Chem. C*, 2011, **115**, 7355-7363.
143. B. Chai, T. Peng, J. Mao, K. Li and L. Zan, *Phys. Chem. Chem. Phys.*, 2012, **14**, 16745-16752.
144. S. Obregón and G. Colón, *Appl.Catal., B*,2014, **144**, 775-782.
145. J. Wang, J. Huang, H. Xie and A. Qu, *Int.J. Hydrogen Energy*, 2014, **39**, 6354-6363.
146. Y. Wang, R. Shi, J. Lin and Y. Zhu, *Energy Environ. Sci.*, 2011, **4**,2922-2929.
147. J. X. Sun, Y. P. Yuan, L. G. Qiu, X. Jiang, A. J. Xie, Y. H. Shen and J. F. Zhu, *Dalton Trans.*, 2012, **41**, 6756-6763.
148. S.W. Cao, X.F. Liu, Y.P. Yuan, Z.Y. Zhang, Y.S. Liao, J. Fang, S. C. J. Loo, T. C. Sum and C. Xue, *Appl. Catal., B*, 2014, **147**, 940-946.
149. L. Ge, F. Zuo, J. Liu, Q. Ma, C. Wang, D. Sun, L. Bartels and P. Feng, *J. Phys. Chem. C*, 2012, **116**, 13708-13714.
150. S.W. Cao, Y.P. Yuan, J. Fang, M. M. Shahjamali, F. Y. C. Boey, J. Barber, S. C. Joachim Loo and C. Xue, *Int. J. Hydrogen Energy*, 2013, **38**, 1258-1266.
151. J. Fu, B. Chang, Y. Tian, F. Xi and X. Dong, *J. Mater. Chem. A*,2013, **1**, 3083-3090.
152. S. C. Yan, S. B. Lv, Z. S. Li and Z. G. Zou, *Dalton Trans.*, 2010, **39**, 1488-1491.
153. S. Ida, A. Takashiba, S. Koga, H. Hagiwara and T. Ishihara, *J. Am. Chem. Soc.*, 2014, **136**, 1872-1878.
154. Q. Huang, F. Kang, H. Liu, Q. Li and X. Xiao, *J. Mater. Chem. A*,2013, **1**, 2418-2425.
155. H. Kim, M. Seol, J. Lee and K. Yong, *J. Phys. Chem. C*, 2011, **115**, 25429-25436.
156. Y. Hou, F. Zuo, A. Dagg and P. Feng, *Nano Lett.*, 2012, **12**, 6464-6473.
157. M. Shi, X. Pan, W. Qiu, D. Zheng, M. Xu and H. Chen, *Int. J. Hydrogen Energy*, 2011, **36**, 15153-15159.
158. Y. Hou, F. Zuo, A. Dagg and P. Feng, *Angew. Chem. Int. Ed.*, 2013, **52**, 1248-1252.
159. Y. J. Hwang, C. H. Wu, C. Hahn, H. E. Jeong and P. Yang, *Nano Lett.*, 2012, **12**, 1678-1682.
160. Y. B. Dou, A. W. Zhou, T. Pan, J. B. Han, M. Wei,D. G. Evans and X. Duan, *Chem. Comm.*, 2014,**50**, 7136-7138.
161. J. Zhang, Y. Wang, J. Jin, J. Zhang, Z. Lin, F. Huang and J. Yu, *ACS Appl. Mater. Interfaces*, 2013, **5**, 10317-10324.
162. A. Thibert, F. A. Frame, E. Busby, M. A. Holmes, F. E. Osterloh and D. S. Larsen, *J. Phys. Chem. Lett.*, 2011, **2**, 2688-2694.
163. L. Huang, X. Wang, J. Yang, G. Liu, J. Han and C. Li, *J. Phys. Chem. C*, 2013, **117**, 11584-11591.
164. X. Yang, J. Xu, T. Wong, Q. Yang and C. S. Lee, *Phys. Chem. Chem.Phys.*, 2013, **15**, 12688-12693.
165. K. Maeda, T. Takata, M. Hara, N. Saito, Y. Inoue, H. Kobayashi and K. Domen,*J. Am. Chem. Soc.*, 2005, **127**, 8286-8287.
166. Q. Liu, Y. Zhou, J. Kou, X. Chen, Z. Tian, J. Gao, S. Yan and Z. Zou, *J. Am. Chem. Soc.*, 2010, **132**, 14385-14387.
167. L. Liu, Z. Ji, W. Zou, X. Gu, Y. Deng, F. Gao, C. Tang and L. Dong, *ACS Catal.*, 2013, **3**, 2052-2061.
168. K. Domen, A. Kudo, T. Onishi, N. Kosugi and H. Kuroda, *J. Phys. Chem.*, 1986, **90**, 292-295.
169. A. Kudo, K. Sayama, A. Tanaka, K. Asakura, K. Domen, K. Maruya and T. Onishi, *J. Catal.*, 1989, **120**, 337-352.

170. J. Ran, J. Zhang, J. Yu, M. Jaroniec and S. Z. Qiao, *Chem. Soc. Rev.*, 2014, **DOI: 10.1039/c3cs60425j**.
171. X. Zong, H. Yan, G. Wu, G. Ma, F. Wen, L. Wang, and C. Li, *J. Am. Chem. Soc.*, 2008, **130**, 7176–7177.
172. T. F. Jaramillo, K. P. Jorgensen, J. Bonde, J. H. Nielsen, S. Horch and I. Chorkendorff, *Science*, 2007, **317**, 100-102.
173. X. Zong, G. P. Wu, H. J. Yan, G. J. Ma, J. Y. Shi, F. Y. Wen, L. Wang and C. Li, *J. Phys. Chem. C*, 2010, **114**, 1963–1968.
174. X. Zong, J. Han, G. Ma, H. Yan, G. Wu and C. Li, *J. Phys. Chem. C*, 2011, **115**, 12202-12208.
175. Y. Hou, A. B. Laursen, J. Zhang, G. Zhang, Y. Zhu, X. Wang, S. Dahl and I. Chorkendorff, *Angew. Chem. Int. Ed.*, 2013, **52**, 3621-3625.
176. W. Zhang, Y. Wang, Z. Wang, Z. Zhong and R. Xu, *Chem. Commun.*,2010, **46**, 7631-7633.
177. M. Tabata, K. Maeda, T. Ishihara, T. Minegishi, T. Takata and K. Domen, *J. Phys. Chem. C*, 2010, **114**, 11215-11220.
178. J. Hong, Y. Wang, Y. Wang, W. Zhang and R. Xu, *ChemSusChem*,2013, **6**, 2263-2268.
179. L. Zhang, B. Tian, F. Chen and J. Zhang, *Int. J. Hydrogen Energy*, 2012, **37**, 17060-17067.
180. J. Wang, B. Li, J. Chen, N. Li, J. Zheng, J. Zhao and Z. Zhu, *Appl. Surf. Sci.*, 2012, **259**, 118-123.
181. Y.P. Yuan, S.W. Cao, L.S. Yin, L. Xu and C. Xue, *Int. J. Hydrogen Energy*, 2013, **38**, 7218-7223.
182. L. Yin, Y.P. Yuan, S.W. Cao, Z. Zhang and C. Xue, *RSC Adv.*, 2014, **4**, 6127-6132.
183. N. A. Assunçào, M. J. de Giz, G. TremiIiosi-FiIho, E. R. Gonzalez, *J. Electrochem. Soc.*, 1997, **144**, 2794-2800.
184. J. Zhang, J. Yu, Y. Zhang, Q. Li and J. R. Gong, *Nano Lett.*, 2011, **11**, 4774-4779.
185. P. Gomathisankar, K. Hachisuka, H. Katsumata, T. Suzuki, K. Funasaka and S. Kaneco, *Int. J. Hydrogen Energy*, 2013, **38**, 8625-8630.
186. L. J. Zhang, T. F. Xie, D. J. Wang, S. Li, L. L. Wang, L. P. Chen and Y. C. Lu, *Int. J. Hydrogen Energy*, 2013, **38**, 11811-11817.
187. J. Santos Cruz, S. A. Mayén Hernández, F. Paraguay Delgado, O. Zelaya Angel, R. Castanedo Pérez and G. Torres Delgado, *Int. J. Photoenergy*, 2013, **2013**, 1-9.
188. K. A. Brown, S. Dayal, X. Ai, G. Rumbles and P. W. King, *J. Am. Chem. Soc.*, 2010, **132**, 9672-9680.
189. K. A. Brown, M. B. Wilker, M. Boehm, G. Dukovic and P. W. King, *J. Am. Chem. Soc.*, 2012, **134**, 5627-5636.
190. J. Huang, K. L. Mulfort, P. Du and L. X. Chen, *J. Am. Chem. Soc.*, 2012, **134**, 16472-16475.
191. C.B. Li, Z.J. Li, S. Yu, G.X. Wang, F. Wang, Q.Y. Meng, B. Chen, K. Feng, C.H. Tung and L.Z. Wu, *Energy Environ. Sci.*, 2013, **6**, 2597-2602.
192. Z. Han, F. Qiu, R. Eisenberg, P. L. Holland and T. D. Krauss, *Science*, 2012, **338**, 1321-1324.
193. J. Dong, M. Wang, X. Li, L. Chen, Y. He and L. Sun,*ChemSusChem*, 2012, **5**, 2133-2138.
194. S. W. Cao, X. F. Liu, Y. P. Yuan, Z. Y. Zhang, J. Fang, S. C. Loo, J. Barber, T. C. Sum and C. Xue, *Phys. Chem. Chem. Phys.*, 2013, **15**, 18363-18366.
195. F. Y. Wen, X. L. Wang and L. Huan, G. J. Ma, J. H. Yang, C. Li, *ChemSusChem*, 2012, **5**, 849-853.
196. S.W. Cao, Y.P. Yuan, J. Barber, S. C. J. Loo and C. Xue, *Appl. Surf.Sci.*, 2014, **DOI: 10.1016/j.apsusc.2014.04.094.**
197. K. Potje-Kamloth, *Chem. Rev.*, 2008, **108**, 367-399.
198. M. Jakob, H. Levanon and P. V. Kamat, *Nano Lett.*, 2003, **3**, 353-358.
199. V. Subramanian, E. E. Wolf and P. V. Kamat, *J. Am. Chem. Soc.*, 2004, **126**, 4943-4950.
200. A. Wood, M. Giersig and P. Mulvaney, *J. Phys. Chem. B*, 2001, **105**, 8810-8815.
201. J. H. Yang, H. X. Han and Can Li, *Acc. Chem. Res.*, 2013, **46**, 1900-1909.
202. S. R. Lingampalli, U. K. Gautam and C. N. R. Rao, *Energy Environ. Sci.*, 2013, **6**, 3589-3594.
203. X. Wu, Q. Song, L. Jia, Q. Li, C. Yang and L. Lin, *Int. J. Hydrogen Energy*, 2012, **37**, 109-114.
204. J. Fang, L. Xu, Z. Zhang, Y. Yuan, S. Cao, Z. Wang, L. Yin, Y. Liao and C. Xue, *ACS Appl. Mater. Interfaces*, 2013, **5**, 8088-8092.
205. S.W. Cao, J. Fang, M. M. Shahjamali, F. Y. C. Boey, J. Barber, S. C.J. Loo and C. Xue, *RSC Adv.*, 2012, **2**, 5513-5515.
206. Y. Sasaki, A. Iwase, H. Kato and A. Kudo, *J. Catal.*, 2008, **259**, 133-137.
207. M. Hara, J. Nunoshige, T. Takata, J. N. Kondo and K. Domen, *Chem. Commun.*, 2003, 3000-3001.
208. S. Trasatti, *J. Electroanal. Chem.*, 1972, **39**, 163-184.
209. Y. Wang, Y. Wang and R. Xu, *J. Phys. Chem. C*, 2013, **117**, 783-790.
210. Z. Hu and J. C. Yu, *J. Mater. Chem. A*, 2013, **1**, 12221-12228.
211. A. K. Agegnehu, C.J. Pan, J. Rick, J.F. Lee, W.N. Su and B.J. Hwang, *J. Mater. Chem.*, 2012, **22**, 13849-13854.
212. W. Wang, S. Liu, L. Nie, B. Cheng and J. Yu, *Phys. Chem. Chem. Phys.*, 2013, **15**, 12033-12039.
213. C.T. Dinh, M.H. Pham, F. Kleitz and T.-O. Do, *J. Mater. Chem. A*, 2013, **1**, 13308-13313.
214. P. D. Tran, L. Xi, S. K. Batabyal, L. H. Wong, J. Barber and J. S. Loo, *Phys. Chem. Chem. Phys.*, 2012, **14**, 11596-11599.
215. H.Y. Lin, H.C. Yang and W.L. Wang, *Catal. Today*, 2011, **174**, 106-113.
216. W. J. Foo, C. Zhang and G. W. Ho, *Nanoscale*, 2013, **5**, 759-764.
217. T. Yui, A. Kan, C. Saitoh, K. Koike, T. Ibusuki and O. Ishitani, *ACS Appl. Mater. Interfaces*, 2011, **3**, 2594-2600.
218. W. N. Wang, W. J. An, B. Ramalingam, S. Mukherjee, D. M. Niedzwiedzki, S. Gangopadhyay and P. Biswas, *J. Am. Chem. Soc.*, 2012, **134**, 11276-11281.
219. K. Sayama and H. Arakawa, *J. Phys. Chem.* , 1993, **97**, 531-533.
220. I. H. Tseng, J. C. S. Wu and H.Y. Chou, *J. Catal.*, 2004, **221**, 432440.
221. Y. Li, W.N. Wang, Z. Zhan, M.H. Woo, C.Y. Wu and P. Biswas, *Appl. Catal., B*,2010, **100**, 386-392.
222. W.N. Wang, J. Park and P. Biswas, *Catal. Sci. Technol.*, 2011, **1**, 593-600.
223. S. Linic, P. Christopher and D. B. Ingram, *Nat. Mater.*, 2011, **10**, 911-921.
224. P. Wang, B. Huang, Y. Dai and M. H. Whangbo, *Phys. Chem. Chem. Phys.*, 2012, **14**, 9813-9825.

225. K. L. Kelly, E. Coronado, L. L. Zhao and G. C. Schatz, *J. Phys.Chem. B*, 2003, **107**, 668-677.
226. H. A. Atwater1 and A. Polman,*Nat. Mater.*, 2010, **9**, 205-213.
227. Y. Tian and T. Tatsuma,*J. Am. Chem. Soc.*, 2005, **127**, 7632-7637.
228. Y. C. Pu, G. Wang, K. D. Chang, Y. Ling, Y. K. Lin, B. C. Fitzmorris, C. M. Liu, X. Lu, Y. Tong, J. Z. Zhang, Y. J. Hsu and Y. Li, *Nano Lett.*, 2013, **13**, 3817-3823.
229. C. Clavero, *Nature photonics*, 2014, **8**, 95-103.
230. A. Furube, L. Du, K. Hara, R. Katoh and M. Tachiya, *J. Am. Chem. Soc.*, 2007, **129**, 14852-14853.
231. A. Furube, L. Du, K. Hara, R. Katoh and M. Tachiya, *J. Phys. Chem. C*, 2009, 113, 6454-6462.
232. J. B. Priebe, M. Karnahl, H. Junge, M. Beller, D. Hollmann and A. Bruckner, *Angew. Chem. Int. Ed.*, 2013, **52**, 11420-11424.
233. C. G. Silva, R. Jua´rez, T. Marino,R. Molinari and H. Garcia, *J. Am. Chem. Soc.*, 2011, **133**, 595-602.
234. J. Long, H. Chang, Q. Gu, J. Xu, L. Fan, S. Wang, Y. Zhou, W. Wei,L. Huang, X. Wang, P. Liu and W. Huang, *Energy Environ. Sci.*, 2014, **7**, 973-977.
235. Z. Bian, T. Tachikawa, P. Zhang, M. Fujitsuka and T. Majima, *J. Am.Chem. Soc.*, 2014, **136**, 458-465.
236. A. Tanaka, S. Sakaguchi, K. Hashimoto and H. Kominami, *ACS Catal.*, 2013, **3**, 79-85.
237. Z. Zhang, A. Li, S. W. Cao, M. Bosman, S. Li and C. Xue, *Nanoscale*, 2014, **6**, 5217-5222.
238. S. Mukherjee, L. Zhou, A. M. Goodman, N. Large, C. Ayala-Orozco, Y. Zhang, P. Nordlander and N. J. Halas, *J. Am. Chem. Soc.*, 2014, **136**, 64-67.
239. Z. Zheng, T. Tachikawa and T. Majima, *J. Am. Chem. Soc.*, 2014, **136**, 6870-6873.
240. A. Tanaka, K. Hashimoto and H. Kominami, *J. Am. Chem. Soc.*, 2014, **136**, 586-589.
241. M. Grzelczak, J. Pe´rez-Juste, F. J. G. de Abajo and L. M. Liz-Marza´n, *J. Phys. Chem. C*, 2007, **111**, 6183-6188.
242. K. Awazu, M. Fujimaki, C. Rockstuhl, J. Tominaga, H. Murakami, Y. Ohki, N. Yoshida and T. Watanabe, *J. Am.Chem. Soc.*, 2008, **130**, 1676-1680.
243. M. K. Kumar, S. Krishnamoorthy, L. K. Tan, S. Y. Chiam, S. Tripathy and H. Gao, *ACS Catal.*, 2011, **1**, 300-308.
244. D. B. Ingram and S. Linic, *J. Am. Chem. Soc.*, 2011, **133**, 5202-5205.
245. Z. W. Seh, S. Liu, M. Low, S. Y. Zhang, Z. Liu, A. Mlayah and M. Y. Han, *Adv. Mater.*, 2012, **24**, 2310-2314.
246. S. K. Cushing, J. Li, F. Meng, T. R. Senty, S. Suri, M. Zhi, M. Li, A. D. Bristow and N. Wu, *J. Am. Chem. Soc.*, 2012, **134**, 15033-15041.
247. W. Hou, W. H. Hung, P. Pavaskar, A. Goeppert, M. Aykol andS. B. Cronin, *ACS Catal.*, 2011, **1**, 929-936.
248. E. Liu, L. Kang, F. Wu, T. Sun, X. Hu, Y. Yang, H. Liu and J. Fan, *Plasmonics*, 2014, **9**, 61-70.
249. K. Maeda, *ACS Catal.*, 2013, **3**, 1486-1503.
250. X. Wang, G. Liu, L. Wang, Z.G. Chen, G. Q. Lu and H.M. Cheng, *Adv. Energy Mater.*, 2012, **2**, 42-46.
251. P. Zhou, J. Yu and M. Jaroniec, *Adv. Mater.*, 2014, **26**, 4920-4935.

Table of Contents

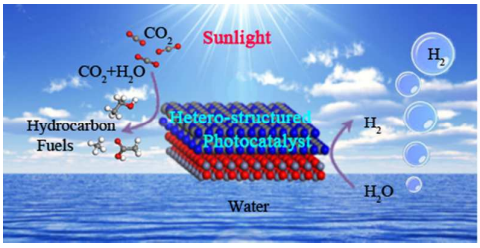

The recent developments of hetero-nanostructures for photocatalytic H_2 production and CO_2 reduction are reviewed in detail based on material compositions that form heterojunctions.